On Nano Size Structures For Enhanced Early Bone Formation

Luiz Meirelles

GÖTEBORGS UNIVERSITET

SAHLGRENSKA AKADEMIN

Department of Prosthodontics / Dental Material Science

Department of Biomaterials

Göteborg 2007

To Cristiane
with love

This thesis represents number 36 in a series of investigations on implants, hard tissue and the locomotor apparatus originating from the Department of Biomaterials/Handicap Research, Institute for Clinical Sciences at Sahlgrenska Academy, Göteborg University, Sweden.

1. **Anders R Eriksson DDS, 1984.** Heat-induced Bone Tissue Injury. An in vivo investigation of heat tolerance of bone tissue and temperature rise in the drilling of cortical bone. Thesis defended 21.2.1984. Ext. examin.: Docent K.-G. Thorngren.
2. **Magnus Jacobsson MD, 1985.** On Bone Behaviour after Irradiation. Thesis defended 29.4.1985. Ext. examin.: Docent A. Nathanson.
3. **Fredrik Buch MD, 1985.** On Electrical Stimulation of Bone Tissue. Thesis defended 28.5.1985. Ext. examin.: Docent T. Ejsing-Jörgensen.
4. **Peter Kälebo MD, 1987.** On Experimental Bone Regeneration in Titanium Implants. A quantitative microradiographic and histologic investigation using the Bone Harvest Chamber. Thesis defended 1.10.1987. Ext. examin.: Docent N.Egund.
5. **Lars Carlsson MD, 1989.** On the Development of a new Concept for Orthopaedic Implant Fixation. Thesis defended 2.12.1989. Ext. examin.: Docent L.-Å. Broström.
6. **Tord Röstlund MD, 1990.** On the Development of a New Arthroplasty. Thesis defended 19.1.1990. Ext. examin.: Docent Å. Carlsson.
7. **Carina Johansson Techn Res, 1991.** On Tissue Reactions to Metal Implants. Thesis defended 12.4.1991. Ext. examin.: Professor K. Nilner.
8. **Lars Sennerby DDS, 1991.** On the Bone Tissue Response to Titanium Implants. Thesis defended 24.9.1991. Ext. examin.: Dr J.E. Davis.
9. **Per Morberg MD, 1991.** On Bone Tissue Reactions to Acrylic Cement. Thesis defended 19.12.1991. Ext. examin.: Docent K. Obrant.
10. **Ulla Myhr PT, 1994.** On Factors of Importance for Sitting in Children with Cerebral Palsy. Thesis defended 15.4.1994. Ext. examin.: Docent K. Harms-Ringdahl.
11. **Magnus Gottlander MD, 1994.** On Hard Tissue Reactions to Hydroxyapatite-Coated Titanium Implants. Thesis defended 25.11.1994. Ext. examin.: Docent P. Aspenberg.
12. **Edward Ebramzadeh MScEng, 1995.** On Factors Affecting Long-Term Outcome of Total Hip Replacements. Thesis defended 6.2.1995. Ext. examin.: Docent L. Linder.
13. **Patricia Campbell BA, 1995.** On Aseptic Loosening in Total Hip Replacement: the Role of UHMWPE Wear Particles. Thesis defended 7.2.1995. Ext. examin.: Professor D. Howie.
14. **Ann Wennerberg DDS, 1996.** On Surface Roughness and Implant Incorporation. Thesis defended 19.4.1996. Ext. examin.: Professor P.-O. Glantz.
15. **Neil Meredith BDS MSc FDS RCS, 1997.** On the Clinical Measurement of Implant Stability and Osseointegration. Thesis defended 3.6.1997. Ext. examin.: Professor J. Brunski.
16. **Lars Rasmusson DDS, 1998.** On Implant Integration in Membrane-Induced and Grafter Bone. Thesis defended 4.12.1998. Ext. examin.: Professor R. Haanaes.
17. **Thay Q Lee MSc, 1999.** On the Biomechanics of the Patellofemoral Joint and Patellar Resurfacing in Total Knee Arthroplasty. Thesis defended 19.4.1999. Ext. examin.: Docent G. Nemeth.
18. **Anna Karin Lundgren DDS, 1999.** On Factors Influencing Guided Regeneration and Augmentation of Intramembraneous Bone. Thesis defended 7.5.1999. Ext. examin.: Professor B. Klinge.
19. **Carl-Johan Ivanoff DDS, 1999.** On Surgical and Implant Related Factors Influencing Integration andFunction of Titanium Implants. Experimental and Clinical Aspects. Thesis defended 12.5.1999. Ext. examin.:Professor B. Rosenquist.

20. **Bertil Friberg DDS MDS, 1999.** On Bone Quality and Implant Stability Measurements. Thesis defended 12.11.1999. Ext. examin.: Docent P. Åstrand.
21. **Åse Allansdotter Johnsson MD, 1999.** On Implant Integration in Irradiated Bone. An Experimental Study of the Effects of Hyberbaric Oxygenation and Delayed Implant Placement. Thesis defended 8.12.1999. Ext. examin.: Docent K. Arvidsson-Fyrberg.
22. **Börje Svensson DDS, 2000.** On Costochondral Grafts Replacing Mandibular Condyles in Juvenile Chronic Arthritis. A Clinical, Histologic and Experimental Study. Thesis defended 22.5.2000. Ext. examin.: Professor Ch. Lindqvist.
23. **Warren Macdonald BEng, MPhil, 2000.** On Component Integration in Total Hip Arthroplasty: Pre-Clinical Evaluations. Thesis defended 1.9.2000. Ext. examin.: Dr A.J.C. Lee.
24. **Magne Røkkum MD, 2001.** On Late Complications with HA Coated Hip Asthroplasties. Thesis defended 12.10.2001. Ext. examin.: Professor P. Benum.
25. **Carin Hallgren Höstner DDS, 2001.** On the Bone Response to Different Implant Textures. A 3D analysis of roughness, wavelength and surface pattern of experimental implants. Thesis defended 9.11.2001. Ext. examin.: Professor S. Lundgren.
26. **Young-Taeg Sul DDS, 2002.** On the Bone Response to Oxidised Titanium Implants: The role of microporous structure and chemical composition of the surface oxide in enhanced osseointegration. Thesis defended 7.6.2002. Ext. examin.: Professor J.-E. Ellingsen.
27. **Victoria Franke Stenport DDS, 2002.** On Growth Factors and Titanium Implant Integration in Bone. Thesis defended 11.6.2002. Ext. examin.: Associate Professor E. Solheim.
28. **Mikael Sundfeldt MD, 2002.** On the Aetiology of Aseptic Loosening in Joint Arthroplasties, and Routes to Improved cemented Fixation. Thesis defended 14.6.2002. Ext. examin.: Professor N Dahlén.
29. **Christer Slotte DDS, 2003.** On Surgical Techniques to Increase Bone Density and Volume. Studies in the Rat and the Rabbit. Thesis defended 13.6.2003. Ext. examin.: Professor C.H.F. Hämmerle.
30. **Anna Arvidsson MSc, 2003.** On Surface Mediated Interactions Related to Chemo-mechanical Caries Removal. Effects on surrounding tissues and materials. Thesis defended 28.11.2003. Ext. examin.: Professor P. Tengvall.
31. **Pia Bolind DDS, 2004**. On 606 retrieved oral and cranio-facial implants. An analysis of consecutively received human specimens. Thesis defended 17.12. 2004. Ext. examin: Professor A. Piattelli.
32. **Patricia Miranda Burgos DDS, 2006.** On the influence of micro-and macroscopic surface modifications on bone integration of titanium implants.Thesis defended 1.9. 2006. Ext. examin: Professor A. Piattelli.
33. **Jonas P Becktor DDS, 2006.** On factors influencing the outcome of various techniques using endosseous implants for reconstruction of the atrophic edentulous and partially dentate maxilla. Thesis defended 17.11.2006. Ext examin: Professor K. F. Moos
34. **Anna Göransson DDS, 2006.** On Possibly Bioactive CP Titanium Surfaces. Thesis defended 8.12. 2006 Ext examin: Prof B. Melsen
35. **Andreas Thor DDS, 2006**. On platelet-rich plasma in reconstructive dental implant surgery. Thesis defended 8.12. 2006. Ext examin Prof E.M. Pinholt.
36 **Luiz Meirelles DDS MSc 2007.** On Nano Size Structures For Enhanced Early Bone Formation. To be defended 13.6.2007. Ext examin:Professor Lyndon F. Cooper.

Abstract

Purpose The general aim of the present thesis was to investigate early bone response to titanium implants modified with nano size structures. Therefore, 1. a model to evaluate titanium implants modified with nano size structures was validated; 2.a suitable detection method of nano size structures was implemented.

Materials and Methods A rabbit model was selected and healing time was 4 weeks in all experiments. A smooth cylindrical implant design was selected in order to control the macro-threads and micro-structures. Thus, early bone response could be related to added nano size structures alone. A stabilization plate was utilized to ensure adequate fixation of the attached implant. Smooth implants were obtained through polishing techniques (electrical and mechanical) and were used as control surfaces and, after relevant modifications, as experimental surfaces. Six surface modifications were investigated: 1. mechanically polished, 2. electropolished, 3. nano hydroxyapatite (HA), 4. nano titania, 5. blasted (TiO_2) and 6. fluoride-modified. The implant surface topography was measured with an interferometer and an atomic force microscope. Surface roughness parameters were calculated and nano size structures dimension and distribution were characterized. Surface morphology was evaluated by scanning electron microscopy. Surface chemical composition was monitored with X-ray photoelectron spectroscopy. The bone response was measured with removal torque tests and histological and histomorphometrical analyses.

Results The model tested to evaluate smooth implants was found adequate. Atomic force measurements combined with image processor analyses software was suitable to characterize nano size structures at the implant surface. Nano HA modified implants enhanced bone formation at 4 weeks of healing compared to electropolished implants. However, placed in a gap healing model the nano HA modified implants showed similar bone formation compared to electropolished implants. If both test and control implants were modified with nano structures, so-called bioactive nano HA and bioinert nano titania, respectively; enhanced bone response of 24% was found to the "bioinert" nano titania implants, although not statistically significant. The beneficial effect of nano size structures on the experimental model was tested on screw shaped moderately rough implants. The oral implants that exhibited particular nano structures (fluoride and nano HA) showed a tendency of higher removal torque values compared to control (blasted) implants, that lacked such structures.

Conclusions Based on *in vivo* animal experiments, enhanced bone formation was demonstrated to smooth and moderately rough titanium implants modified with nano size structures with different chemical composition.

Key words: nano structures, nanotopography, surface modification, osseointegration, bone tissue, titanium implants

ISBN: 978-91-628-7202-1

Correspondence: Luiz Meirelles, Dept Biomaterials, Box 412, 405 30 Göteborg, Sweden; email: luiz.meirelles@odontologi.gu.se

List of papers

This thesis is based on the following papers, which are referred to in the text by their Roman numerals (I-V):

Paper I: *validate the model*
Meirelles L, Arvidsson A, Albrektsson T, Wennerberg A. Increased bone formation to unstable nano rough titanium implants.
Clin Oral Impl Res, In press.

Paper II: *effect of nano HA*
Meirelles L, Arvidsson A, Andersson M, Kjellin P, Albrektsson T, Wennerberg A. Nano hydroxyapatite structures influence early bone formation.
Submitted for publication.

Paper III: *nano HA in a gap model*
Meirelles L, Albrektsson T, Kjellin P, Arvidsson A, Stenport Franke V, Andersson M, Wennerberg A. Bone reaction to nano hydroxyapatite modified titanium implants placed in a gap healing model.
J Biomed Mater Res Part:A, accepted.

Paper IV: *nano- HA and titania*
Meirelles L, Melin, L, Peltola T, Kjellin P, Kangasniemi I, Fredrik C, Andersson M, Albrektsson T., Wennerberg A. Nano size hydroxyapatite and titania nano structures and early bone healing.
Submitted for publication.

Paper V: *nano structures on oral implants*
Meirelles L, Currie F, Jacobsson M, Albrektsson T, Wennerberg A. The effect of chemical and nano modifications on early stage of osseointegration.
Submitted for publication.

Contents

Introduction

Background

The replacement of lost or failing tissues demands artificial substitutes that should be suitable for every patient and could be delivered and stored. Implant material and design have been in focus of intense research to optimize tissue response to foreign materials. The replacement of a single lost tooth requires adequate function of a multi-unit implant. Successful connection between hard and soft tissues and the inserted implant is a vital requirement for long-term outcome. In addition to the implant material and design, effort of researchers and clinicians have been concentrated to the surgical procedure, minimizing trauma and optimizing implant stability.
Osseointegrated commercially pure (c.p.) titanium implants were successfully introduced by Brånemark et al[1] for rehabilitation of edentulous jaws. Later, good results with the Brånemark implant system were reported by Brånemark et al[2] and Albrektsson et al[3] at longer healing periods. Attempts to explain the mechanisms behind osseointegration started in the 1980s; bone response to different metal alloys[4], implant designs and surgical fit[5], were investigated at different healing periods and with different techniques[6]. The aim was to evaluate bone-implant interface interactions that may lead to failure or success of implant rehabilitation. The concept developed to restore fully edentulous jaws was also applied for fixed partial bridges or single replacements where long term evaluations likewise demonstrated high degree of success[7,8]. Today, c.p. titanium is the most widespread used biomaterial in oral implantology and titanium based materials are used for replacement of lost tissues in several parts of the human body.

Despite high success rates obtained with the correct protocol, some cases may not be ideal for repair with osseointegrated implants. Factors underlying implant success or failure have been investigated in numerous scientific reports. However, the mechanisms that explain the background to success or failure are not fully understood. At this moment, nanotechnology has emerged with several techniques to modify implant surfaces. In addition, some evaluation techniques at the nano level are contributing important information regarding tissue and cell interactions with the implanted material. Increased knowledge of the early healing events at the nano level may help to understand the sequence of events at bone-implant interfaces and provide guidelines for the further development of osseointegrated implant surfaces.

Bone tissue

Bone tissue can be divided in organic and inorganic components, which corresponds to 20% and 65% of the wet weight of bone, respectively. Water content contributes with 10%, approximately. The bone organic matrix is formed mainly by collagen type I and small amounts of type V and XII (90%, approximately). The remaining 10% of the organic matrix is formed by a variety of non-collagenous proteins that have different functions on the regulation of bone mineralization, organization of the matrix and activity of bone cells. The proteins include osteocalcin, osteonectin, bone sialoproteins, bone phosphoproteins and proteoglycans.
The inorganic matrix serves as an ion reservoir and gives bone most of its stiffness and strength. The basic unit of the inorganic matrix is the apatite crystals that contain calcium, phosphorous, sodium and magnesium.
On the macroscopical level there are two types of bone: cortical and cancellous. Cortical and cancellous bone have the same matrix composition and structure, but the mass of the cortical bone matrix per unit of volume is higher, with approximately 10% of porosity compared to 50-90% porosity found in the cancellous bone. This difference in tissue arrangement provides increased resistance to torsion and bending to the cortical compared to the cancellous bone.
At the microcospical level, cortical and cancellous bone may consist of woven or lamellar bone. Woven bone has an irregular pattern of collagen fibrils and it contains approximately four times the number of osteocytes per unit of volume compared to lamellar bone. Osteocytes present in the woven bone vary in size, orientation and distribution, while those in lamellar bone are relatively uniform in size, with the long axis parallel to the collagen fibrils of the matrix. The surfaces of bone are covered with connective tissue sheets called periosteum (externally) and endosteum (internally). The periosteum contributes an important part of the blood supply to the bone and exhibits mesenchymal cells that may differentiate and form osteoblasts and osteocytes. The references consulted in this section includes: Junqueira & Carneiro [9], Buckwalter et al [10] and Bilezikian et al [11].

Bone cells

There are four cells directly responsible for bone formation and resorption through life. *Osteoblasts, bone lining cells and osteocytes* are derived from mesemchymal stem cells; located at the bone marrow and at the perio/endo-steum. They are responsible for the bone matrix deposition and maintenance. *Osteoclasts* are derived from the fusion of bone marrow-derived mononucleated cells and, when active, resorbs bone matrix.
The osteoblast is the key cell for bone formation and it arises from the osteoblast lineage with recognizable stages of proliferation and differentiation, as detected by in vivo and in vitro experiments. There are 7 postulated steps observed from the precursor stem cells to the final osteocyte. The cell development sequence was routinely characterized by morphological definitions, where decreasing profilerative capacity and increasing differentiation was observed.

Morphological definitions are now routinely supplemented by the analysis of bone cell macromolecules, such as bone matrix proteins: type I collagen, osteocalcin (OCN), osteopontin (OPN), bone sialoproteins (BSP); and transcriptors factors, such as: Cbfa1/Runx2, AP-1, Msx-2 and Dlx-5. The expression of each one of these markers is related to differentiation step of the bone cell lineage[12]. In addition, the intensity detected of each marker may indicate how active the cell is; that, ideally, could determine the ability of the cell to form bone on the seeded surface.

The mature osteoblasts are located on the surface of the bone, packed tightly against each other, separated by the mineralized bone by a thin zone called osteoid. An active osteoblast has a round, oval or polyhedral form and secrete the bone matrix, starting with collagen type I. After secretion of several bone matrix components, some osteoblasts are trapped in bone matrix and become osteocytes. The last step of the osteogenic cells may include also cell apoptosis or differentiation to *bone lining cells*.

Bone lining cells are flat, elongated and inactive cells that cover bone surfaces; they do not participate in bone formation or resorption. They have few cytoplasmatic organelles and little is known regarding the function of these cells.

Osteocytes lie in the lacunae situated between lamellae of the matrix. Only one osteocyte is found in each lacuna. Thin canaliculi house cytoplasmatic processes that communicate among osteocytes and molecules are exchanged. Compared to osteoblasts, the almond-shaped osteocytes exhibit significantly reduced number of organelles. These cells are involved in the maintenance of the bone matrix, and their death may be followed by matrix resorption.

The *Osteoclast* has the only function to resorb mineralized tissue, a normal function for bone growth and remodeling. At present, osteoclasts seems to be the only cell that is able to resorb the mineralized tissue matrix, where the larger cells are more effective than the smaller ones. Osteoclasts originate from the hematopoetic tissue. After proliferation and differentiation due to several cytokines and growth factors, the mononuclear preosteoclasts are guided to bone surfaces. At the resorption site is observed the retraction of the bone lining cells and the multinuclear osteoclast can attach to the mineralized border. The resorbing osteoclasts are highly polarized cells, containing several different plasma membrane domains: ruffled border, sealing zone, basolateral domain and a functional secretory domain. The ruffled border is the actual resorbing unit of the cell, characterized by a low pH. Osteoclasts can go through more than one resorption cycle after which they can go two different routes: fission into mononuclear cells or death.

Bone chemistry of the inorganic matrix

The mineral part of bone is formed by hydroxyapatite, $Ca_{10}(PO4)_6(OH)_2$. Hydroxyapatite crystal precursors are initially found inside matrix vesicles; extracellular vesicles associated with mineralized tissue forming cells, such as osteoblasts and odontoblasts. Ca^{2+} and PO_4^{3-} accumulation inside these matrix vesicles will form noncrystalline amorphous calcium phosphates

further transformed to hydroxyapatite (Phase 1). Some reports indicate that this transitory amorphous phase is characterized by octacalcium phosphate[13]. Continuous growth of the crystals inside the matrix vesicles will expose them to the extracellular fluid, after penetrating the matrix vesicle membranes (Phase 2)[14]. The HA crystals are deposited in a way that their *c* axes are aligned to the collagen fibril[15] and will act as nucleation sites for the continuous bone mineralization process. The intimate relationship between the HA crystals and the collagen fibers was demonstrated in the early 1950s[16].

When investigated in more detail, the apatite present in bone is rather variable (as expected from biological material). In the early 1950s, McConnell[17] speculated that bone mineral is more similar to carbonate containing apatite, a notion supported by others[18,19]. The overall content of CO_3 in the apatite structure may be related to the age of the tissue[20]. Some others elements, such as, F, Cl, Mg, Na and K may be found in bone, dependent on the age of the host, biopsy region and species investigated. Legeros[21] suggested the approximate formula for the mineral phase of bone to be: $(Ca, Mg, Na)_{10}(PO_4HPO_4CO_3)_6(OH)_2$.

Bone 3D nanotopography

Bone may be represented by different levels of organization; from the macro to the nano structure, i.e. from the overall shape of each individual bone till small structures at the nano level (Fig.1). Bone extracellular matrix (ECM) is mainly formed by collagen type I and apatite crystals, constituents of the organic and inorganic matrix, respectively. Both collagen type I and apatite crystal dimensions are in the nanometer size, producing a unique 3D nano topography. Collagen type I is formed by the arrangement of cylindrical triple helix units with an average diameter of 1.5 nm and length of 300 nm[22], that forms collagen fibrils of 80-100 nm in diameter. The triple helix cylinder molecules of collagen are parallel, organized in different rows and separated by the following cylinder by a gap of 35 nm. The apatite crystals present in bone exhibit a plate-shaped form, with average dimensions of 50 X 25 X 4 nm, evaluated by TEM[23] and small angle X-ray scattering[24], respectively.

Cells attachment, migration, proliferation and protein syntheses are affected by the three-dimensional spatial arrangement of the ECM, which provides binding sites on the different nano structures existent.

The importance of the existent 3D nano topography of bone does not imply that chemical signaling is irrelevant. Cell-cell and cell-matrix chemical signaling follows binding sites located in the different structures located on the extracellular matrix[25,26]. The issue highlighted is that the adequate understanding of the bone ECM topography may indicate the adequate 3D nano topography for biomaterials surfaces. The characterization of 3D nanotopography may not only focus on the early events during tissue healing after implantation; on load bearing implants, such as the osseointegrated implants, the surface may interact favorably during function, i.e., enable proper stress transfer at the implant-tissue interface, withstanding the dynamic shear strengths.

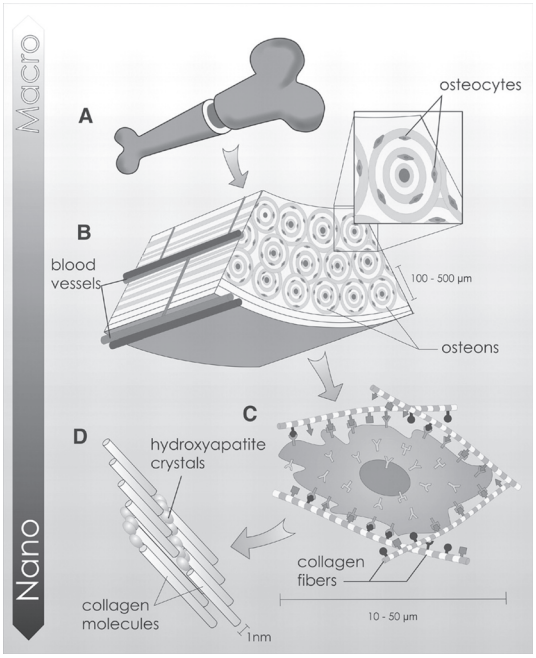

Figure 1. Hierarchical organization of bone at different size levels in bone. Overall shape of bone (a) at the macro level; each osteon formed by the osteocytes on the micro level (b), apatite crystals and collagen fibers with the binding sites represent the structures at the nano level of resolution, forming the 3D nano topography of bone (c,d). From [Stevens, M; George, J. Exploring and engineering the cell surface interface. Science 2005; 310:1135-38]. Reprinted with permission from AAAS.

Bone response and biomaterials classification

Bone response

The bone tissue response to osseointegrated implants can be related to six factors proposed by Albrektsson and coworkers[27]: implant material, implant design, surface quality, status of the bone bed, surgical technique and implant loading conditions. The improvement of the osseointegrated implant success may be result of increased knowledge of these factors.

Biomaterial classification

At about the same time as the work by Albrektsson et al[27], Osborn & Newesely [28], proposed a classification of materials to be implanted in the bone according to the material activity and related tissue response: *biotolerant, bioinert, bioactive*. According to this classification:

A ***biotolerant*** material was described as capable of a distance osteogenesis; bone will form but not in contact with the host bone. The implant retention is based on the principle of interlocking exclusively by mechanical means. The materials included in this group are represented by bone cement, stainless steel and Cr-Co alloy.

A ***bioinert*** material was supposed to show contact osteogenesis; direct contact of the adjacent bone is observed to the implanted material. The implant retention is also based on the interlocking principle, i.e. exclusively by a mechanically based anchorage. The materials included in this group are represented by carbon, alumina and titanium.

Bioactive materials showed bonding osteogenesis; direct chemical bond between implant and adjacent bone occur. The implant retention is based on both mechanical interlocking and chemical bonding between bone-implant. The materials included in this group are represented by glass-ceramics, tricalcium phosphates and hydroxyapatite.

Implant Surface in Relation to Bone Healing

There are different methods and materials currently in use to optimize the bone response and other approaches are under evaluation. For example, surface modifications, such as: heat treatment, blasting, acid etching, hydroxyapatite coating and sol-gel coating have been introduced.

Heat treated implants

Hazan and coworkers evaluated Ti-6Al-4V and stainless steel implants[29]. The Ti-6Al-4V screw implants were heat treated at 280°C for 180 min and compared to non-heated Ti-6Al-4V implants, placed in the femur medullary canal of rats. Evaluation periods included 4, 5, 6, 10 and 35 days and significantly increased pull out values for the heat treated implants were reported at all time periods evaluated. However, the increased bone formation to heat treated implants reported by Hazan et al[29] was not observed in a more recent study[30]. Titanium c.p. implants that were heat treated up to 700-800°C and when compared to controls exhibited thicker oxide and similar roughness parameters. Bone response after 6 weeks in the rabbit tibia and femur demonstrated similar values of bone contact and bone area. An alternative approach to improve surface affinity for bone was previous treatment with *NaOH* of the surface before heat treatment[31]. The NaOH treatment results in a sodium titanate hydrogel, converted in an amorphous sodium titanate layer with heat treatment at 600°C [32]. In vivo tests revealed increased bone response to the alkali-heat treated compared to untreated implants after 3-12 weeks of healing in rabbits[33] and dogs[34]. However, the authors did not evaluate the surface topography, and the clear difference observed in porosity may be enough to explain the higher bone formation to the alkali-heat treated implants. In another study[35], a porous implant served as control and was also further modified with apatite-wollastonite (AW) glass and with alkali- heat treatment. Hence, the clear difference in microtopography observed in the previous studies[33,34] was not present. In this study[35], where all the implants exhibited surface pores, no difference in bone ingrowth after 4 and 12 weeks healing period was observed when the so-called bioactive was compared to the control implant. Push out tests revealed higher value only between the control and alkali-heat treated implant after 4 weeks, whereas similar values were reported after 12 weeks.

Blasted implants

The grit blasting technique usually is performed with titania or alumina particles. The final surface roughness may be controlled by varying the particle size selected. Titanium implants blasted with alumina and titania particles with sizes of 25 μm and 75 μm (S_a = 1-1.5 μm) demonstrated enhanced bone formation compared to turned implants (S_a = 0.4 μm) placed in

rabbits[36]. TioBlast implants (AstraTech) surface modification included grit blasting with titania particles. The success rate of TioBlast implants reported in a prospective study after 7 years was 96.9% with the same survival rate at 10 years. Compared to turned implants, TioBlast implants demonstrated lower bone loss and higher overall success rates[37,38]. Grit blasting represented the first clinically applied surface modification of titanium implants; the technique has then been further modified with acid etching, such as: SLA (Straumann) and Osseospeed (AstraTech).

Acid Etched implants

Acid etching of titanium removes the oxide layer and parts of the underlying material, even if the surface oxide immediately reforms under normal conditions. The extent of material removed depends on the acid concentration, temperature and treatment time. The most commonly used solutions for acid etching of titanium includes: a mixture of HNO_3 and HF or a mixture of HCl and H_2SO_4[39]. Fluoride treatment has been investigated in the field of biomaterials field due to the benefits of this element in bone physiology. An in vitro analysis of fluoride modified implants was performed with human mesenchymal cells. No difference in cell attachment[40,41] was detected between the fluoride modified and control (grit-blasted) implants. In addition, decreased cell proliferation was observed after 7 days on the fluoride modified compared to control (grit-blasted) implants[41]. The results of osteoblast differentiation showed increased expression of Cbfa1[40,42], osterix[40] and bone sialoprotein[41] to fluoridated implants. An in vivo evaluation was performed to test the potentially enhanced bone response to fluoride modified implants. Ellingsen (1995)[43] used an aqueous solution with up to 4% of NaF for etching titanium c.p. coined-shape implants. After 4 and 8 weeks the push out test revealed an improved retention for the NaF treated implant compared to control (untreated) implants. Moreover, improved bone formation was observed on screw shaped implants treated with diluted HF solution[44]. Analyses were performed after 1 and 3 months. Fluoride modified implants exhibited increased bone contact and bone area values at both periods evaluated compared to the control implants. Removal torque evaluations showed higher values for the fluoride implants after a 3-month healing period, but no difference at 1 month. Enhanced bone formation was reported at an earlier healing period of 21 days[41]. In this study[41], implants were placed in the rat tibia, and showed increased bone contact values for the fluoride modified implants compared to the control (untreated) implants.

Hydroxyapatite coated implants

Hydroxyapatite is one of the materials that may form a direct and strong binding between the implant and bone tissue[45,46], named as bioactive according to Osborn & Newesely[28]

classification. This property of hydroxyapatite, $Ca_{10}(PO4)_6(OH)_2$, is related to a sequence of events that results in precipitation of a CaP rich layer on the implant material through a solid-solution ion exchange on the bone-implant interface[47,48]. This reaction will occur simultaneously with biomolecules incorporation and cell recruitment. The CaP incorporated layer will gradually be developed, via octacalcium phosphate[49], in a biologically equivalent hydroxyapatite[46,50] that will be incorporated in the developing bone[46,51,52].

Synthetic hydroxyapatite has also been widely investigated for biomaterials applications due to the similar chemical composition when compared to the mineral (inorganic) matrix of bone, which is generally referred to as hydroxyapatite. Different elements, such as: F and Si, may be introduced in the synthetic apatite. The presence of different elements in the apatite crystal is of great importance for the surface kinetics of the synthetic material that ultimately is related to bone response. The dissolution rate of the material depends on the particle size, porosity, specific surface area and crystallinity. For example, when comparing to hydroxyapatite; the carbonate apatite is less stable and the fluoride apatite is more stable[53,54]. The decreased dissolution rate of carbonate apatite has been attributed to the simultaneous increase in particle size, evaluated by TEM[55]. It was observed that a higher content of carbonate was associated to an increased particle size. Thus, increased dissolution rate may be related not only to the chemical composition, but also be associated to the difference in particle size.

Depending on the fabrication technique, hydroxyapatite may show a similar crystal structure as the mineral phase of bone. The hydroxyapatite properties known already by early 1980s resulted in an intense investigation for the potential application of the material. HA bulk material was first used for alveolar ridge augmentation[56,57] and craniofacial reconstructive surgery[58]. Further evaluation of bulk HA as a load-bearing implant[59,60] failed in long-term and fractured due to fatigue failure of the ceramic material. The low shear strength of bulk HA required a different approach, where the material was applied as coating on metals. Initially promising results in the late 1980s were reported from different groups in animal experiments[61,62]. The coat was based on the plasma spraying method[63].

HA coatings techniques

Important factors for the behavior of the HA coatings include: chemical composition, Ca/P ratio, crystallinity, microstructure, adhesive strength, thickness and presence of trace elements[64]. Different methods have been described for applying hydroxyapatite coatings onto metals and different material properties may result from each method.

Plasma-spraying is the most important commercially used technique for coating metals, especially titanium. In a so-called plasma gun, an electric arc current of high energy is struck between a cathode and an anode. An inert gas is directed through the space between these electrodes, and the arc current ionizes the gas and a plasma is formed[65]. The rapidly moving

particles present in the plasma are accelerated towards the cathode and anode and then collide with others atoms. The high speed flame with melted particles is directed to the material surface and the ceramic powder is deposited. Initial reports suggested that a chemical bond would occur between the ceramic deposited and the titanium oxides[66]. However this chemical bond was never proven to exist. Plasma spraying technique results in a coating thickness of minimally 40-50 µm. Furthermore, this technique lacks in stability of the deposited ceramic and an amorphous phase is a common finding. It may also be difficult to have a homogenous coating layer on samples with complex design. *In vivo* results showed a faster bone integration in short-term evaluations, however longer evaluation periods failed to maintain the increased bone response values[67-70]. Moreover, some complications have been reported on load bearing implants placed in humans due to de-attachment of the ceramic coating from the bulk metal[71-74].

Spark anodizing is a method based on the principle of anodic oxidation of the metal, a well known method to increase oxide thickness of the metal. In contrast to the anodizing process where the voltage is kept below the dielectric breakdown, spark anodizing is carried out at voltages above the breakdown limit[39]. The thickness of the oxide produced may vary from a few up to 20 µm. If calcium and phosphate are added to the solution, the oxide formed will incorporate such elements, but not as hydroxyapatite[75]. Hydrothermal post-treatment has proven effective in converting the non crystalline calcium phosphate in the oxide into crystalline hydroxyapatite[76]. An adhesion strength of 38-40 MPa was achieved with a low electrolyte concentration that lead to an incomplete coverage of the implant by HA crystals and lower bone response, when compared to implants with full HA coverage[76,77]. Even when compared to turned implants, the spark anodized with HA crystals failed to show increased bone formation[78]. So far, no implants have been placed in humans with this modification.

HA thin coatings techniques (< 10 µm)

Pulsed laser deposition is a method with well controlled thickness of the coating. The number of laser pulses determined the desired film thickness, deposited at a rate of approximately 0.02 nm/laser shot. The crystalline phases of CaP formed, Ca/P ratio and coating adhesion are dependent on the temperature and gas content in the vacuum chamber. Interestingly, the coating thickness used for in vitro an in vivo tests was 2,0 µm[79,80], a thickness that may lead to the undesirable de-attachment. So far, no implants have been placed in humans with this modification.

Sputter deposition is a process that ejects atoms or molecules of a material by bombardment of high energy ions. There are several sputter techniques and a common drawback inherent in all these methods is that the deposition rate is very low and the process itself is very slow[81]. The deposition rate is improved by using a magnetically enhanced variant of diode sputtering, so-called radiofrequency magnetron sputtering[82]. In vivo evaluation at short- and long- term

periods revealed more bone contact compared to amorphous CaP and turned implants[83,84]. However, no implants have been clinically documented with this surface modification.
The *Sol-gel* method has been successfully used to deposit hydroxyapatite thin films on titanium samples with different designs, such as discs, cylinders and screws[85,86]. The thickness may vary from 1 to 10 μm. Coating thickness can be controlled during the different stages of the sol-gel process or by simply adding different number of layers on the substrate. The low bond strength observed on sol-gel derived HA layers [86] may be improved by mixing TiO_2 sol with HA sol, producing a HA-TiO_2 composite sols[87]. The sol-gel method may produce different ceramics of interest for osseointegrated implants, different from HA, as will be discussed in the next section.

Sol-Gel coated implants

The sol-gel method represents a simple and low cost procedure with homogenous chemical composition onto substrates with large dimensions and complex design. Sol-gel processing of inorganic ceramic and glass materials started at the mid 1800s[88], when it was reported that hydrolysis of tetraethyl orthosilicate formed SiO_2. However, at that time, extremely long drying periods (1 year or more) were necessary and consequently there was little technological interest. The development of new evaluation techniques from the 1950s, for example: nuclear magnetic resonance and X-ray photoelectron spectroscopy enabled the investigation of each step of the sol-gel process on the nanometer scale. The better understanding and control of each step of the sol-gel process allowed a remarkable decrease in the drying step without damage to the coating[89]. The sol-gel method has attracted great attention in the field of biomaterials since the final product may include hydroxyapatite and titania, two of the most common materials used for osseointegrated implants. Sol-gel titania films may be prepared using a dip coating[90,91] or spin coating[92] process. Titania bonding strengths of the films are related to the surface pre-treatment, firing atmosphere, and surface topography[93]. Moreover, the particle size and particle aggregation can be modulated by the aging time of the sol; that may produce different coating thickness, ranging from 210 to 380 nm[94]. In addition, the number of layers applied onto the sample affects the surface topography. A more narrow peak distance distribution was demonstrated with 5 layers compared to 1 layer[95].
In vivo bone tissue evaluations of surfaces modified using the sol-gel method have been mainly performed on CaP or glass materials. Bone formation was in close contact with the material and no adverse reaction was observed[96,97]. However, the behavior of sol-gel modifications of loaded osseointegrated implants in the long term remains unknown.

Topography

The modifications currently available for osseointegrated implants, and generally in use, are a variation of physical and/or chemical methods. Most often a chemical modification also results in different surface chemistry, surface energy and surface charge. In addition, some modifications, like HA coated implants, possess surface properties that distinguish them from turned implants, besides the obvious difference in surface chemistry and microtopography. In this section, topographical modification experiments performed by several authors were considered, even when a chemical method was used. However, the potential variables besides the difference in surface topography highlighted by the authors should be kept in mind. Implant surface topography may be divided in: macro, micro and nano level of resolution, as represented by Figure 2.

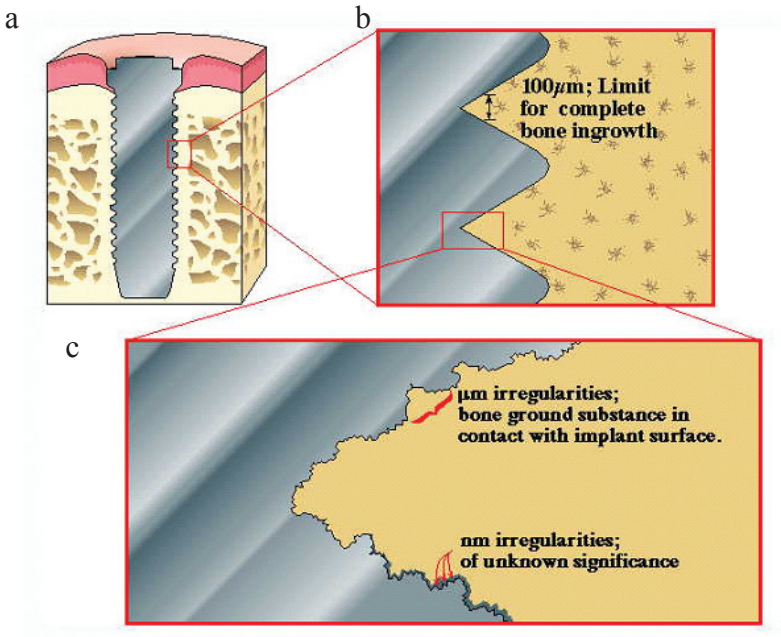

Figure 2. Implant macro level represented by the overall shape and thread design (a,b). Micro and nano structures are observed at higher resolution (c). From [Wennerberg A. On surface roughness and implant incorporation. PhD thesis. Göteborg: Göteborg University; 1996] Reprinted with permission by the author.

Micro topography

In vitro

Surface microtopography has been reported to influence cell adhesion, morphology, proliferation and differentiation. Bowers et al[98] investigated osteoblast attachment on c.p. titanium discs. Higher cell attachment was observed on the sand blasted discs after 30-, 60- and 120 minutes compared to smoother surfaces, that were polished and acid etched. Similar results were reported by Keller et al[99]. Osteoblast like cells attachment was evaluated on c.p. titanium discs with different surface roughness. A tendency for higher osteoblast like cell attachment for the rougher (sandblasted) surfaces compared to smooth (polished) surfaces after 15-, 30- and 60 minutes was observed. After 120 minutes, there was a significant increase of cell attachment on the rougher sandblasted (R_a=0.9 μm) compared to smoother surfaces polished with 600 grit SiC paper (R_a=0.2 μm) and the smoothest one polished with 1μm diamond paste (R_a=0.04 μm). Cell attachment does not represent the entire cell activity on implants. Cell activity on surfaces may also be demonstrated by the differences in cell proliferation and gene expression. Boyan et al[100] evaluated osteoblast like cells on turned (R_a=0.6 μm), grit-blasted/acid etched (R_a=4.0 μm) and plasma sprayed (R_a=5.2 μm) surfaces. Cell morphology was similar after 14 days on the different surfaces. In addition, calcium and phosphorous content did not vary with the surface roughness, whereas cell proliferation decreased as the surface roughness increased. In contrast, alkaline phosphatase activity was increased with increasing roughness. Masaki et al[40] evaluated the gene expression of bone ECM proteins and transcription factors of human mesenchymal cells on: 1. TiO_2 grit blasted (S_a=1.1μm) surfaces, 2. (1) + acid etched in dilute HF solution (S_a=0.9 μm) surfaces, 3. grit blasted Al_2O_3 + acid etched in H_2SO_4/HCl and 4. (3) prepared under N_2 atmosphere and stored in NaCl. The S_a values of the surfaces 1and 2 were reported from a previous study[44] and the S_a values of the surfaces 3 and 4 were not reported. After 72 h, no difference in osteocalcin, bone sialoprotein II and collagen type I expression were detected among the investigated surfaces. In contrast, Cbfa1 and osterix expression was higher on surfaces 1 and 2; and ALP gene expression was higher on surface 4, compared to the other surfaces.

In vivo

Several reports evaluated bone formation to implants with different surface roughness, measured as bone contact to the implant surface and/or biomechanical tests of the bone-implant interface. Generally, rougher implants show enhanced bone formation compared to smoother implants[101-104]. Titanium implants surface microtopography was firstly described with 3D roughness parameters in 1992[105]. Later, blasted implants with different 3D roughness parameters were evaluated in a series of studies[106-109] and an optimal surface range of roughness was suggested for S_a values between 1-1.5 μm[36] . The continued increase of surface roughness

above this range was not correlated with correspondent increase of bone response, on the contrary, the opposite was the case. Today, most currently available dental implants exhibit a moderately rough implant surface, with 3D surface roughness values within the optimal range as suggested by Wennerberg & Albrektsson[110].

Nano topography

In this thesis nano topography will be separated in two sub headings: *Nano Roughness and Nano Features*, which could have been applied to microtopography (previous section) as well. However, the literature concerning surface micro topography generally refers to surface roughness, not referring to individual features with micro dimensions present at the material surface. The nano topography literature commonly refers to both *nano roughness* and to specifically designed nano features added on the material surface, so called *nanofabricated* materials. It is important to understand that the overall surface roughness parameters of the sample will be modified when features are added on the surface i.e., by adding nano features, the surface roughness will be modified as well. Moreover, the nano rough materials may also possess nano features; however, the modification used to produce the so-called nano rough materials did not intentionally produce such nano features and, from the surface roughness parameters described is not possible to evaluate the dimension of each individual feature at the surface. In contrast, nano fabricated features have well defined dimensions that aim to modulate cell activity. Specific cell response, such as: attachment, migration, proliferation and differentiation can be obtained guided by the features present at the surface.

Nano Roughness

In vitro Webster et al[111] evaluated osteoblast adhesion on alumina and titania discs prepared by compacting powders with different particles size onto the surface. The discs were sintered at different temperatures to obtain different nano roughness parameters of alumina and titania materials. Significantly increased osteoblast adhesion was observed on alumina discs with increased root mean square deviation (S_q) of 20 nm compared to 17 nm and larger surface area of 1.73 compared to 1.15 μm^2, respectively. Furthermore, the titania discs revealed increased osteoblast adhesion to discs with increased surface roughness (32 and 12 nm, respectively) and larger surface area (1.45 and 1.07 μm^2, respectively). In addition, discs prepared with an identical method, but the powders consisting of Ti, Ti_6Al_4 and CoCrMo were tested. As previously reported for alumina and titania discs, increased osteoblast adhesion was found in the discs from the three groups with increased S_q values[112]. Webster et al[113] investigated osteoblast adhesion and type and concentration of different proteins adsorbed on the surface. The materials included were: alumina, titania and HA, with different nano roughness. Pore diameter and porosity (%) were also calculated. As previously reported, the

osteoblast adhesion was greater on the discs that exhibited increased nano roughness, independent of the different surface chemistry. Surface porosity was higher and pore diameter decreased on the discs with increased nano roughness. Protein adsorption revealed greater amount of vitronectin associated to the increased osteoblast adhesion on the nano rougher implants. The osteoblast proliferation and ALP synthesis on these surfaces was evaluated on another study from the same group[114]. Osteoblast proliferation increased in all tested discs (alumina, titania and HA) with increased nano roughness after 3 and 5 days. In addition, ALP synthesis was higher after 21 and 28 days on the discs with increased nano roughness values. Oliveira & Nanci[115] cultured new bone rat calvaria cells on titanium discs etched with H_2SO_4 and H_2O_2. The acid etched surface revealed nano pits, whereas the control (turned) surfaces failed to show such features, although the surface roughness was not numerically evaluated. The results indicated an overexpression of OPN and BSP both intra- and extracellulary. In addition, a higher proportion of cells was observed with peripheral cytoplasmic distribution of OPN as early as 6h.

Nano Features

The literature cited in the following section will include nano feature modifications that exhibit at least one dimension below the 100 nm limit. The first commonly investigated design[116,117], with controlled dimensions on the surface, was the parallel *groove and ridge* arrangement at the micro level of resolution. Cell orientation was related to the groove orientation, described as the *contact guidance* phenomenon. The methods currently in use enable the fabrication of features with well controlled dimensions within the nanometer level. However, the groove and ridge arrangements are not in use for metal implants with complex designs, even if important findings on cell activity have emerged from these investigations. Wojciak-Stothard et al[118] investigated murine macrophages on flat and nano grooved surfaces with different depths. Fifteen minutes after plating, most cells remained rounded on the plain substrata compared to well spread cells observed on the nano grooved substrata, which indicates cell activation. Moreover, cell adhesion increased gradually from the plain substrata to the shallow (30 nm) grooved substrata with higher values observed on the deepest (282 nm) grooved substrata. Similar results were found for cell orientation; the deeper the grooves the more orientated the cells. Readers interested in a more detailed explanation of the importance of groove and ridge dimensions on cell activity and orientation are directed to review papers in the field (Curtis & Wilkinson[119]; Flemming et al[120]).

Another approach to optimize cell activity with nano features include the so-called *islands*[121,122] or *hemispherical pillars*[123,124], achieved by polymer demixing processes or colloidal lithography. Dalby et al[121] compared fibroblast activity on flat surfaces and surfaces with 13 nm high islands of a diameter of 263 nm. After 3 days, increased fibroblast spreading, more focal contacts associated to vinculin, upregulation of genes involved with cell signaling and collagen precursors were observed on the surfaces with nano islands compared to the flat surfaces. In

another study[122], endothelial cell activity was tested on surfaces with islands with heights of 13-, 35- and 95 nm. Similar to fibroblasts [121], endothelial cells on the surfaces with 13nm islands revealed the largest cell areas (longer and wider axes) and a well defined cytoskeleton, compared to the flat and to the 35- and 95 nm island surfaces. Contrary to the increased activity of the fibroblast and endothelial cells, surfaces with similar features (18-, 35 and 95 nm height islands) did not influence rat calvaria bone cells[125]. In a recent paper, Dalby et al[126] compared cell activity on surfaces with different nano features, including 35- and 45 nm height islands with a diameter of 2.2 μm and 1.7 μm, respectively. Features with column shape with 10 nm height and 144 diameter were added on the flat (control) substrata. The human bone marrow cells showed an increased cell spreading on all the three groups with nano features compared to flat substrata, with cells extending filopodia towards the nano features. It was also demonstrated a well defined cytoskeleton, enhanced expression of stress fibers with clear focal contacts, and increased expression of osteocalcin and osteopontin on the substrata with nano features.

The most used material at present for nano fabrication is silicon or polystyrene (tissue culture plastic). These materials are cheap and very easy to work with due to several chemical reactants available. However, silicon and polystyrene do not have the mechanical properties required to load bearing osseointegrated implants. Recently, a modification with defined nano size crystals was implemented on titanium samples, through the sol-gel route. Zhu et al[127] prepared nano HA crystals of 15-50 nm in length and coated turned and anodized titanium plates. Mouse pre osteoblast cells had decreased adhesion after 15 min on the nano HA coated surface and similar values after 30 min compared to the control (uncoated) implants. Nano HA showed well developed filopodia and lamellipodia compared to the control implants; that demonstrated a greater number of focal contacts. The size of the nano crystals was not evaluated on the surface. Therefore, the size of the features present at the surface is unknown. Sato et al[128] reported the dimensions of the nano HA crystal of 40-100 nm in length and diameter of 20-30 nm. However, SEM and laser particle size analyses revealed crystal agglomerations and broad size distribution, resulting in features up to 10 μm at the surface. Thus, the use of precursor materials with nano sizes may not ensure the equivalent size on the final surface.

There is clear evidence from numerous in vitro studies that cell activity can be modulated by nano size structures of different dimensions and distribution at the surface. However, there is no evidence of modulation of in vivo bone tissue response to implants due to nano size surface structures alone.

Aims

1. To validate a model for evaluation of bone healing to smooth cylindrical titanium implants

2. To investigate the influence of nano size hydroxyapatite structures on early bone formation

3. To determine the effect of nano size hydroxyapatite structures on early bone formation in a gap healing design

4. To compare early bone formation to titanium implants with nano size "bioactive" and "bioinert" surfaces

5. To investigate the early bone formation to moderately rough screw shaped implants with nano size structures of different chemical compositions

Material and Methods

Implant Design

In study I, II, III and IV cylindrical implants were turned from c.p. titanium (grade 3) rods with a diameter of 3.5 mm and length of 8.0 mm. In study I, test implants had a threaded top to ensure full fixation on the stabilization plate, whereas the control implants had a cylindrical design from the bottom to the top. In study II-IV, all the implants had the same design as the test implant from study I.

In study V, screw-shaped blasted implants were used (Astra Tech AB, Mölndal, Sweden). Implants were turned from c.p. titanium (grade 3) rods and further blasted with TiO_2.

Surface Modifications

A total of three underlying topographies have been used in this thesis: 1 mechanical polished, 2 electropolished and 3 TiO_2 blasted. Further implant surface modifications included nano HA (Promimic, Göteborg, Sweden), fluoride-modified (Astra Tech AB, Mölndal, Sweden), and nano titania (Vivoxid, Turku, Finland). In study I, surface modification included only mechanically polished implants. Study II and III included electropolished implants further modified with nano HA. Study IV included mechanically polished implants modified with nano hydroxyapatite and nano titania. Study V included TiO_2 blasted implants further modified with nano hydroxyapatite, and fluoride acid etching.

Table1. Implant design, underlying surface and nano modification investigated in each study.

	Implant design	Underlying surface	Nano modification
Study I	Cylindrical	Mechanically polished	none
Study II	Cylindrical	Electropolished	Nano HA
Study III	Cylindrical	Electropolished	Nano HA
Study IV	Cylindrical	Mechanically polished	Nano- HA and titania
Study V	Screw shaped	TiO_2 blasted	Fluoride and nano HA

Stabilization Plate

Experimental cylindrical implants used in study I-IV lack of macro and micro retention. Therefore, a stabilization plate was implemented to ensure implant stability during healing phase. The plate consists of two side holes for the fixating screws and a threaded central hole for the tested implants. This model provides the same fixation to the implant no matter the surface properties and prevents uncontrolled micromovements that may cause soft tissue integration of the very smooth implant used in this study. The stabilization plate was originally developed to ensure maximal stability enabling in vivo observations of the microcirculation of grafted bone[129].

3D Topographical Characterization

Interferometer- Micrometer Level of Resolution

The principle of the interferometer is that two light waves, when brought together, interfere with each other. If the crest of one wave coincides with the trough of the other, the interference is destructive and the waves cancel out. On the other hand, if two crests or two troughs coincide, the waves reinforce each other. Subsequently, an optical fringe with parallel light and dark bands will be formed. A MicroXam equipment (PhaseShift, Tucson, USA) was used for interferometry evaluation of the implant surface topography with a measurement area of 200X260 μm. The equipment has a lateral resolution of 0.3 μm and vertical resolution of 0.05 nm. The maximum vertical measuring range is 5 mm. The instrument is suitable to evaluate structures at the micrometer level of resolution in height and spatial direction and at the sub-nanometer level of resolution in height direction.

AFM – Nanometer Level of Resolution

AFM characterization was used to evaluate the implant surface with a resolution at the nanometer level. In contrast to the interferometer principle, AFM measurements require contact between a scanning probe and the surface. AFM principle depends on the selected operating modes: 1 constant height, 2 constant force and 3 intermittent contact (Tapping mode™). The AFM in the present thesis used the Tapping mode™. A cantilever is attached to a piezo crystal which oscillates in the vertical direction in the range of 100-400 kHz. When the tip comes close to the sample, the oscillation of the cantilever is damped. The oscillation of the cantilever is monitored by a photo diode. The equipment has a lateral resolution of 2 nm and a vertical resolution in the atomic level i.e, picometer level of resolution. AFM analysis was performed in TappingMode™ using etched silicon probes (Digital Instruments, Santa Barbara,

USA) with cantilever lengths of 125 nm and a resonance frequency of 290 kHz. Measurement areas of 10x10 μm, each consisting of 512 scans, was recorded and the images were captured at a scan rate of 1.0 Hz.

Filter Selection

The raw data obtained from the topographical equipments were further processed to separate the form, waviness and roughness from the original measurements. A Gaussian high pass filter (50X50 μm) was used in all the optical interferometer measurements in study I-V. The Gaussian filter is suitable for smoothing surfaces with rich features. In the AFM measurements small surface corrugations can sometimes be dominated by the noise in the scanner system. This will create observable steps between the scan lines. A least mean square (LMS) fit method substracts a fitted polynomial function from each individual scan line with a defined polynomial degree. Therefore, in the AFM measurements a third order LMS fit line-wise correction was selected. However, there might be less information about corrugations perpendicular to the scan lines and especially for roughness measurements, this may cause underestimated values[130].

3D Topographical parameters

3D surface roughness parameters can be separated into four groups depending on the characteristics of the surface that they quantify, according to Stout[131].

1. Amplitude parameters.
2. Spatial parameters.
3. Hybrid parameters.
4. Functional parameters.

In the present thesis one of the amplitude, hybrid and spatial parameters were used to describe the surface roughness, as recommended by Wennerberg & Albrektsson[110]. S_a amplitude parameter is the arithmetic average height deviation, S_{dr} hybrid parameter is the developed surface area ratio and S_{ds} spatial parameter is the number of local maxima per area.

Surface features characterization

In addition to the surface roughness calculation, the AFM images were evaluated with an image processor (SPIP™, Image Metrology, Lyngby, Denmark), to detect pore and feature dimensions with the grain/pore mode. The threshold segmentation method of detecting the grains/pores was selected in the present thesis. The method defines a threshold level and a binary condition is imposed. In the grain analysis mode, only part of the signal above the threshold is considered a segment/grain to be detected and the rest is disregarded. Alternatively, the parts under the threshold level can be interpreted as the segments to be detected, which will be considered as pores (Fig. 3).

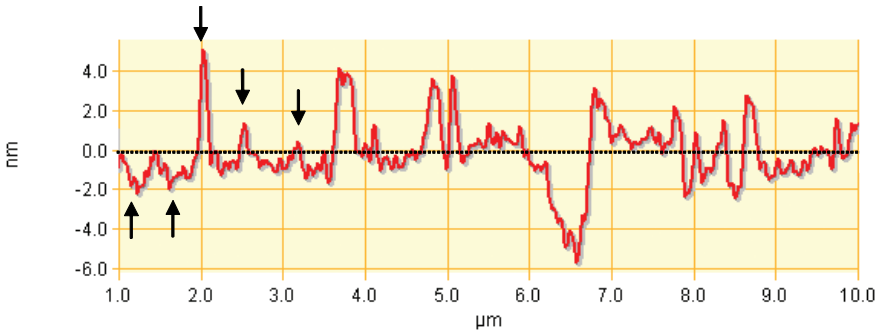

Figure 3. 2D profile of AFM measurement (10x10 µm). The black dashed line represents the detection level. In the grain analysis mode, the structures above (↓) the detection level will be counted. In the pore analysis, the structures below (↑) the detection level will be counted.

Chemical Characterization

Chemical composition of the implants was monitored by X-ray photoelectron spectroscopy (XPS). The principle of the XPS is the emission of photoelectrons from atoms by absorption of photons excited by a X-ray beam. This observed photoelectron emission peaks in the spectrum are due to the different energy levels in the originating atoms from the material surface. These levels known as binding energies are element specific and represent the basis for the analytical application of the XPS. The measurement is performed under ultra high vacuum and provides qualitative and semi-quantitative information on the elemental composition of the sample. The instrument used was a PHI 5500 (Perkin Elmer, Physical Electronics Division) with a monochromatic Al Kα X-ray source operated at 350 W. The relative energy scale was fixed with C 1s.

Animal Model and Anaesthesia

All studies were approved by the local ethic committee at the Göteborg University. A total of fifty New Zealand white rabbits of both sexes were used in the experiments. All animals were adult, aged from 9 to 11 months, only female rabbits were used, except for study V, where only male rabbits were used. The animals were kept in separate cages before surgery and two to three days after implant surgery. Thereafter, all the animals were kept in a specially designed room. In study V, the male rabbits were kept in separate cages during the experiment. All animals had free access to tap water and were fed with standard pellets, carrots, apples and hay. One animal died in study II one day after surgery, when re-suturing was been applied.
Animals were anaesthetized with intramuscular injections of fentanyl and fluanison (Hypnorm Vet, Janssen Farmaucetica, Belgium) at a dose of 0.5 mL per kg of body weight and intraperitoneal injections of diazepam (Stesolid, Dumex, Denmark) at a dose of 0,25 mg per animal. If necessary anaesthesia was maintained using additional doses of Hypnorm at a dose of 0.1 mL per kg body weight. Before surgery, the shaved skin of the rabbit was carefully washed with a mixture of 1% iodine and 70% ethanol. Local anesthesia with 1.0 mL of 5 % lidocaine (Xylocain, Astra Zeneca, Sweden) was injected subcutaneously in the surgical site. A single dose of prophylactic antibiotic (Borgal, Intervet, Boxmeer, The Netherlands) was administered at a dose of 0.5 mL per kg body weight. All ten animals received 0.5 mL of an analgesic (Temgesic, Reckitt and Coleman, England) at a concentration of 0.3 mg/mL on the day of operation and 3 days there after. Four weeks after surgery the animals were anaesthetized with intramuscular injections of fentanyl and fluanison (Hypnorm Vet, Janssen Farmaucetica, Belgium) at a dose of 0.5 mL per kg of body weight and further sacrificed with 10 mL overdose of pentobarbital 60 mg/mL, (Pentobarbitalnatrium, Apoteksbolaget, Sweden).

Surgical technique and implant insertion

Operation was performed under aseptic conditions. In study I-IV, three holes were drilled on the flat proximal medial tibial methaphysis surface parallel to the long axis of the bone. This procedure was done under copious saline irrigation at low rotatory speed. A 3.5 mm drill was utilized to prepare the central hole for the cylindrical implant in study I,II, IV, whereas in study III a 4.2 mm drill was used. Thereafter the stabilization plate was anchored by two fixating screws of 1.0 mm in diameter through the side holes fastened against the cortical bone. The implant and stabilization plate were already connected before surgery and the instrument used to handle the implant-plate gripped the plate; not the implant. This ensured a safe handling of the implant by the surgeon avoiding contact with the surface. In study V the screw-shaped implants were placed in a randomized design enabling the insertion of one implant of each of the four tested implants group, inserted according to AstraTech protocol.

Bone Response Evaluation Methods

Qualitative Evaluation

In study I, three developing stages of bone formation was observed: primitive woven bone, woven bone and lamellar cortical bone. Primitive woven bone was not fully mineralized and darkly stained, representing the earlier stage of woven bone. Woven bone showed a mineralized matrix, lightly stained than the primitive woven bone, and exhibited a clear distinguishing tissue border. Cortical lamellar bone corresponds to the original cortex of the animal; displays mineralized pale stained matrix and osteocytes parallel to the lamellae. In studies II-V, the qualitative evaluation showed mainly cortical lamellar bone and woven bone. Therefore, no different bone developing stages were described.

Histomorphometric evaluation

A total of 86 implants were prepared for histological analyses. All the implants from study I-IV and 8 implants placed proximally in the right tibia from study V were selected for histological analyses. The implants with surrounding tissues were removed en bloc and immersed in 4% neutral buffered formaldehyde and embedded in light curing resin (Technovit 7200 VLC, Kulzer Wehrhein, Germany). Preparations of undecalcified cut and ground sections from the implants were performed with a sawing and grinding equipment . A central section was taken from each sample and ground to an approximately 40 µm thick section and stained with toluidine blue, as described by Donath[132]. Histological examinations were performed with a light microscope (Eclipse 600, Nikon, Japan) and histomorphometry evaluations were performed in an image software analysis. The implant length and bone area quantifications were performed with aid of a detection threshold colour tool from the software (Image Analysis 2000, Tekno Optik AB, Sweden). The threshold level varies the intensity of black (extreme left) to white (extreme right) of each one of the three colours (Fig. 4). In study I-V bone contact percentage was measured along the entire implant. In study I-IV, bone area percentage was measured inside a region of interest (ROI), drawn as a rectangle with a height of 150 µm from the implant surface. The sequence for bone contact and bone area measurements is shown in Figures 5 and 6.

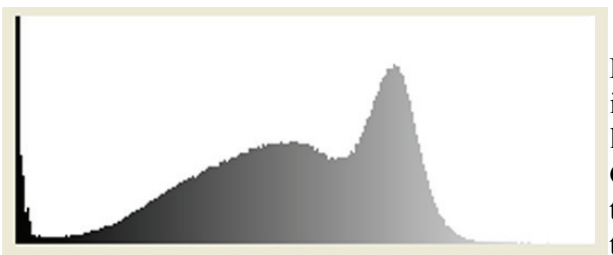

Figure 4. Luminance histogram of the image shown in figures 5 and 6; from the left (darker) to the right (lighter). The Red-Green-Blue colours are superimposed over this histogram, producing the different tones of each colour.

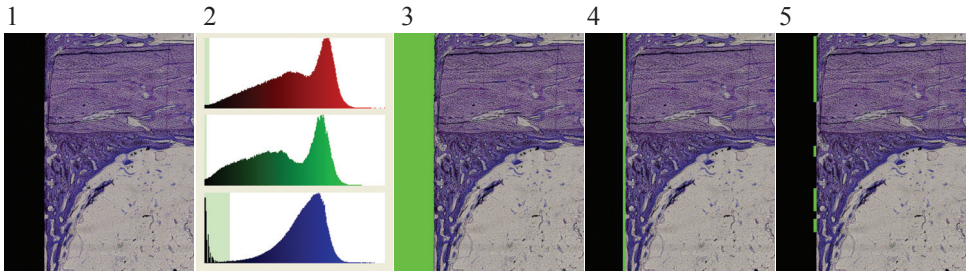

Figure 5. Sequence for bone-implant contact measurements. The first step is to select the titanium implant on the colour threshold tool (2) from the original image (1). Titanium implant is visualized here as pure black, where the threshold level of the red-green-blue colors for black is on the extreme left of the diagram. The titanium implant area is marked as green (3). Next, the outer line of the implant was separated from the implant area marked and counted as the implant length (4). Finally, the bone contact areas were manually marked and the bone contact percentage calculated (5).

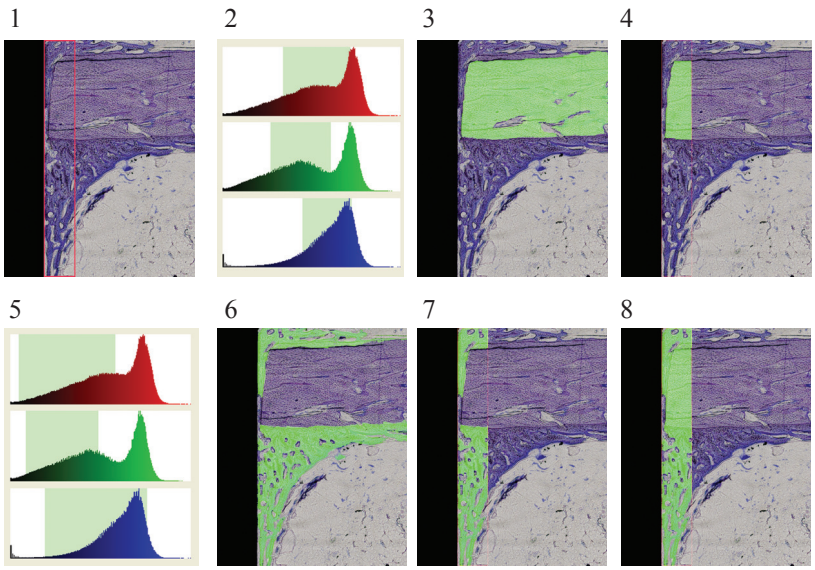

Figure 6. Sequence for bone area measurements. The first step is to select a region of interest (ROI), where the bone area will be calculated (1). The second step is selecting the range of the three colors in the threshold color tool that combined will produce the desired final color (2). The cortical lamellar bone on the entire image is marked (3) and the bone area percentage can be calculated inside the ROI (4). Further, the same sequence was followed for the woven bone (5-7), whereas the threshold level was shifted and enlarged to the left side (5), compared to the threshold observed on the cortical lamellar bone (2). Finally, the marked cortical lamellar bone and woven bone inside the ROI percentage is combined in the same image (8), allowing the calculation of bone area percentage. To obtain separately the values of each "type" of bone observed, bone area measurements can be performed in step 4 and 7.

Removal torque test

The biomechanical test of the implant-bone interface was performed with the removal torque (RTQ) test in 32 implants in study V. The RTQ instrument is an electronic equipment (Detektor AB, Gothenburg, Sweden) involving a strain gauge transducer used for testing the implant stability (the peak loosening torque in Ncm) in the bone bed and thus can be regarded as a three dimensional test roughly reflecting the interfacial shear strength between bone tissue and the implant . A linearly increasing torque is applied on the same axis of the implant until failure of integration is reached, and the peak value recorded.

Statistics

Wilcoxon sign rank test was selected for bone contact and bone area evaluation in studies I-IV. Kruskal-Wallis test evaluated the interferometer surface roughness parameters within each group in study II. In study I-IV, the surface roughness comparison between the two groups was performed with Mann-Whitney test. In study V, RTQ values were analyzed with the Kruskal-Wallis test. Differences were considered statistically significant at $p \leq 0.05$.

Results

3D Topographical Characterization

Interferometer – Micrometer Level of Resolution

The titanium cylinders implants used in the study I-IV evaluated with interferometer revealed a very smooth surface, achieved by different surface treatments. In study I and IV polishing lines were observed, shallower after the nano coating on study IV. In study II and III the electropolishing technique produced a very smooth surface and the grain boundaries could be observed on the implants. In study V, all the implants showed a moderately rough implant surface. The measurement area evaluated in all implants was 200X260 μm. Surface roughness parameters calculated were the following: S_a; S_{ds}; S_{dr}. A summary of the surface roughness parameters of the implants used in study I-V is presented in Table 2.

AFM – Nanometer Level of Resolution

The measurements at higher resolution level revealed in more detail the structures observed with the interferometer and some structures not detected with the previous equipment. In study I and IV the polishing lines were observed with the AFM as seen with the interferometer. Moreover, in study IV, nano structures were detected at the valleys and ridges of the nano HA coated implant, whereas the nano titania implants exhibited a homogenous layer over the surface, with rare shallow remaining polishing lines visible. In study II and III, the AFM measurements of the very smooth implants exhibited the titanium grain boundaries, as seen with the interferometer, and no groove-ridge background was detected. The nano structures were observed at the surface on a similar plane. The measurement area was 10X10 μm in all studies. The surface roughness parameters S_a, S_{ds} and S_{dr} of the titanium cylindrical implants used in the study I-IV, evaluated at higher resolution with AFM, is summarized in Table 3.

Surface features and pore characterization

The structures present at the implant surface detected with AFM measurements in study II-IV was characterized as pores; below the detection level determined, and as features; above the threshold level determined. The structure characterization was performed with an image processor (SPIP™, Image Metrology, Denmark), that provides automatic detection of each

individual structure. In study II both pores and features were evaluated. In study III only pores were evaluated, whereas in study IV only the features were evaluated. The surface feature and pore characterization values are presented in Table 4. To better describe the features present in study II and IV, a frequency histogram was plotted with all detected elements. In study II the diameter frequency histogram was similar for the electropolished and electropolished-HA implants, but with some few more features detected in the range of 200-300 nm on the electropolished-HA implant. In study IV, a narrow distribution is observed on the frequency histogram of height and diameter of the titania implant, with some feature diameters up to 100 nm and heights of 4 nm; the HA implant had some features with diameters up to 380 nm and heights of 40 nm, with some intermediate values shown as well. The features detected on the grain mode of a nano HA coated implant are shown in Figure 7.

Chemical Characterization

All test implants evaluated in studies II and IV consisted mainly of TiO_2. Carbon surface contaminants were present in similar content among the implants evaluated, due to air exposure. Some traces of N were present in all implants investigated. The test nano HA implant (Study II, V) contained Ca and P ions on the XPS survey spectra. In study V, the fluoride etched implant contained small amounts of fluoride anions.

Bone Response

Qualitative Evaluation

In all five studies, overall bone formation was similar to the implants. New formed bone could be observed in the endosteal and periosteal regions, and lining the implant surface (endosteal formation); and between the plate and the stabilization plate (periosteal formation) in study I-IV. The origin of newly formed bone was the cortical lamellar bone of the animal. In study I, a primitive woven bone formation was observed mainly on the unstable implant compared to the stable implant.

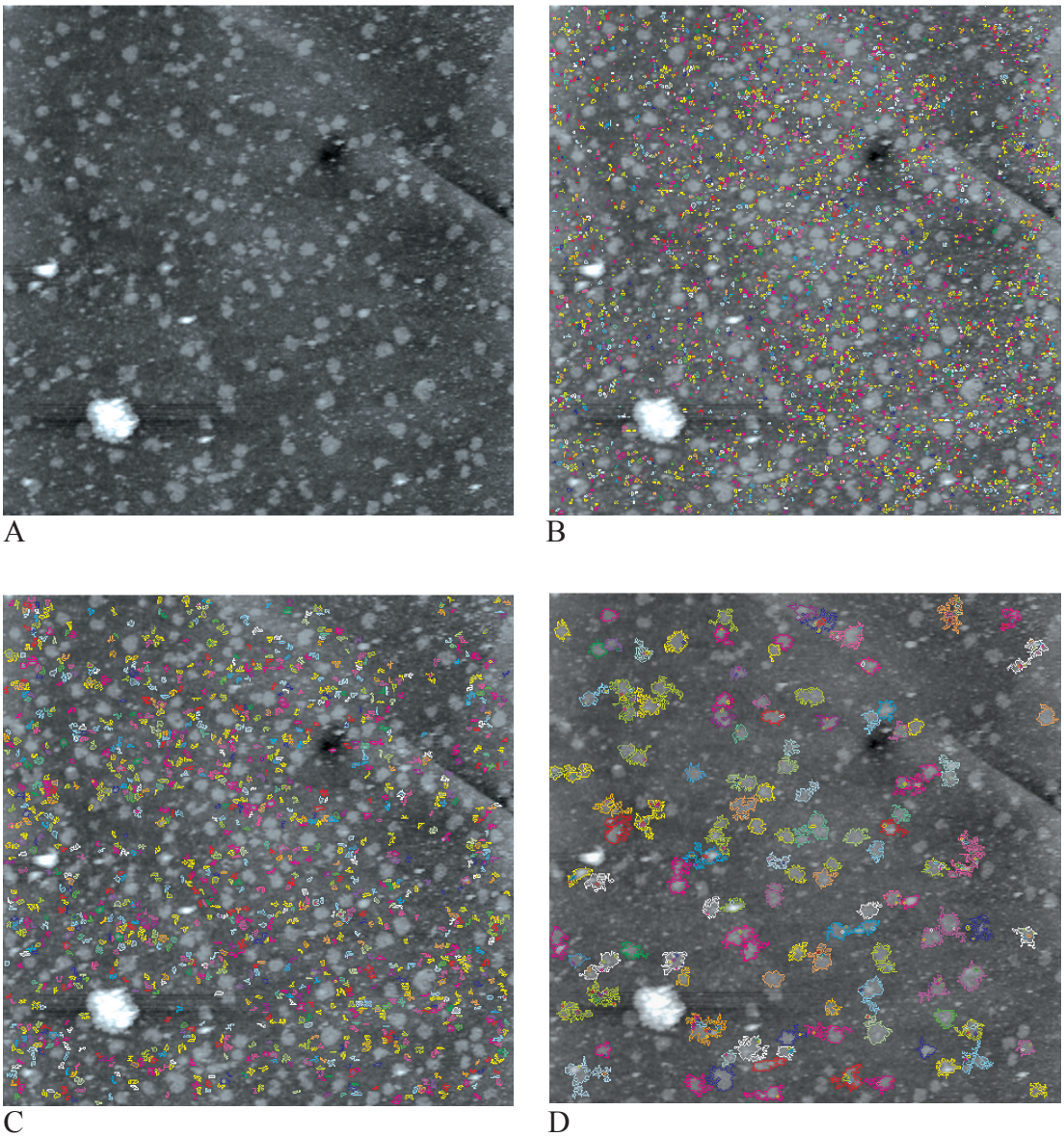

Figure 7. Nano features detected on an electropolished titanium implant modified with nano HA. 2D image of the AFM measurement (10x10 μm) (A). The detection of the features may be performed on a specific dimension range set before the calculation. Here, this was done to make the features visualization more clear. Feature length of < 100 nm, 200-300 nm and 400-1000 nm are marked in B, C, D, respectively.

Table 2 Interferometer evaluation. A summary of the surface roughness on the different surface modifications used in study I, II, III, IV and V. The errors of tilt and bow were removed with Gaussian high pass filter (50x50 µm). A measurement area of 200x260 µm was used.

		Interferometer											
		Study I	**Study II**		**Study III**		**Study IV**			**Study V**			
		Polished	E	E-HA	E	E-HA	HA	Titania		B	B-HA	B-F1	B-F2
S_a	(nm)	109	94	134	49	84	170	121	(µm)	1.42	1.36	1.26	1.24
S_{ds}	(μm^{-2})	0.1	0	0	0	0	0.1	0.1	(mm^{-2})	0.1	0.1	0.1	0.1
S_{dr}	(%)	2.2	0.1	0.3	0	0.1	2.6	1.6	(%)	30.1	30.3	29.2	28

Study I- implants were mechanically polished (polished). Study II and III- electropolished implants non modified with nano HA (E) and modified with nano HA (E-HA). Study IV- implants were mechanically polished and modified with nano HA (HA) and with nano titania (Titania). Study V, blasted (B) implants were modified with nano HA (B-HA) and, two identical groups modified with dilute HF solution (B-F1 and B-F2).

Table 3 AFM evaluation. A summary of the surface roughness on the different surface modifications used in study I, II, III and IV. The errors of tilt and bow were removed with a third order least mean square fit. A measurement area of 10x10 µm was used and the images were captured at a scan rate of 1.0 Hz.

	AFM						
	Study I	**Study II**		**Study III**		**Study IV**	
	Polished	E	E-HA	E	E-HA	HA	Titania
S_a (nm)	11.7	0.9	2.3	1	1	21.9	9.8
S_{ds} (µm^{-2})	18.4	115	90	154	132	18.2	19.7
S_{dr} (%)	0.7	0	0.4	0.1	0.1	3.1	0.3

Table 4 A summary of the features and pore characterization on the AFM measurements of the different surface modifications used in study II, III and IV. The errors of tilt and bow were removed with a third order least mean square fit. Measurement area of 10x10 µm. Feature diameter (diam.), height, coverage area (cov.) and density (d.); pore diameter (diam.), depth, porosity (por) and number of pores are described, mean (SD).

		Feature				**Pore**			
	Implant	**diam.**	**height**	**cov. (%)**	**d. (n/µm^2)**	**diam.**	**depth**	**por. (%)**	**pores**
Study II	E	61 (40)	1.1 (0.2)	48	104	152 (283)	2.6 (1.2)	2.3	29
	E-HA	67 (54)	1.2 (0.3)	43	90	83 (79)	1.3 (0.4)	7.2	669
Study III	E	-	-	-	-	108 (150)	1.9 (0.5)	2.3	89
	E-HA	-	-	-	-	96 (103)	1.8 (0.3)	2.2	148
Study IV	HA	30 (48)	3 (6)	23	94	-	-	-	-
	Titania	24 (15)	1 (0)	45	721	-	-	-	-

Histomorphometric Evaluation

The healing time was 4 weeks for all studies. In study I, significantly higher bone contact values of 8.6% was found to the unstable implant compared to 4.1 % of the stable implant, whereas bone areas were similar (Fig. 8).
In study II, electropolished implants were compared to electropolished implants modified with nano-HA. A statistically significant difference was found; higher values were observed to the nano size modified implant. The bone contact mean value was 9.0% for the E-HA implant and 3.2% for the E implant. Bone area values were similar in the cortical and endosteal regions (Fig 9).
Electropolished implants with and without nano HA were evaluated placed in a gap model, with a bone defect of 0.35 mm (study III). No significant differences were observed in bone contact and bone area mean values (Fig. 10).
In study IV, where both implants were modified with nano size structures (nano titania and nano hydroxyapatite), bone contact mean value measured on the lateral wall of the implant was 21% for the nano titania and 17% for the nano HA (Fig 11). There was no statistical difference, although an increase of approximately 24% is observed for the nano titania compared to the nano HA. The bone area values were identical (Fig. 11).
In study V, the histological evaluation was performed on 8 implants (2 implants/group) placed proximally in the right tibia. Screw shaped blasted implants that possesed nanostructures revealed bone contact values of 30.4% for the fluoride etched group 1; 27.1% for the fluoride etched group 2; 35.8% for the nano HA, where the bone contact value for the control implant was 21.5 %.

Removal torque test

Removal torque tests were performed on 32 screw shaped implants (8 implants/group) from study V, while the remaining 2 implants from each group was selected for histological analyses. The implants that exhibited nano size features revealed an increase of 17% to 25% of removal torque values compared to the control (blasted) implants, however not statistically significant after 4 weeks. The mean peak value was 29-, 34-, 36-, and 37 Ncm for the control, fluoride 1, fluoride 2 and nano HA surfaces, respectively (Fig. 12).

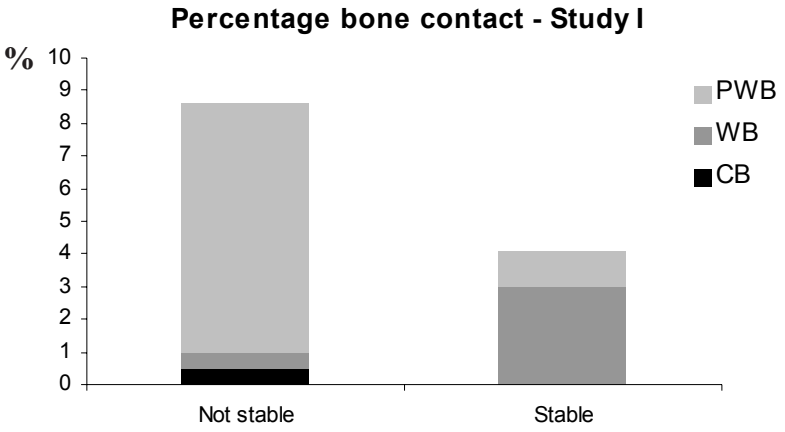

Figure 8 A. The percentage of bone contact in study I. Primitive woven bone (PWB), woven bone (WB), cortical lamellar bone (CB).

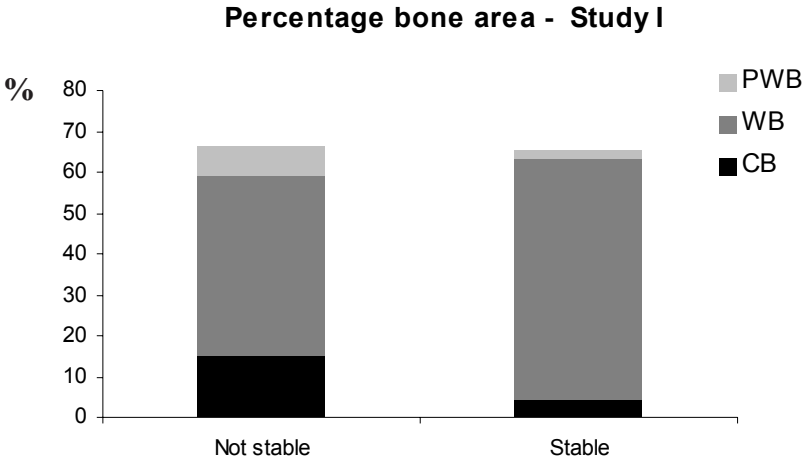

Figure 8 B. The percentage of bone area in study I. Primitive woven bone (PWB), woven bone (WB), cortical lamellar bone (CB).

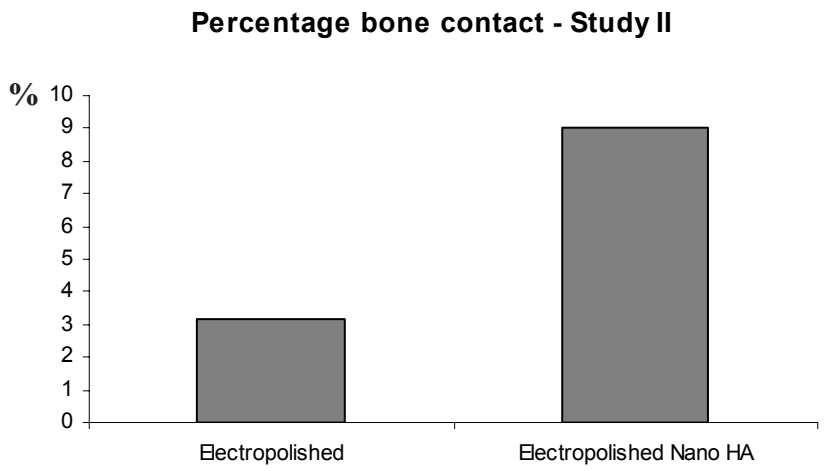

Figure 9 A. The percentage of bone contact in study II.

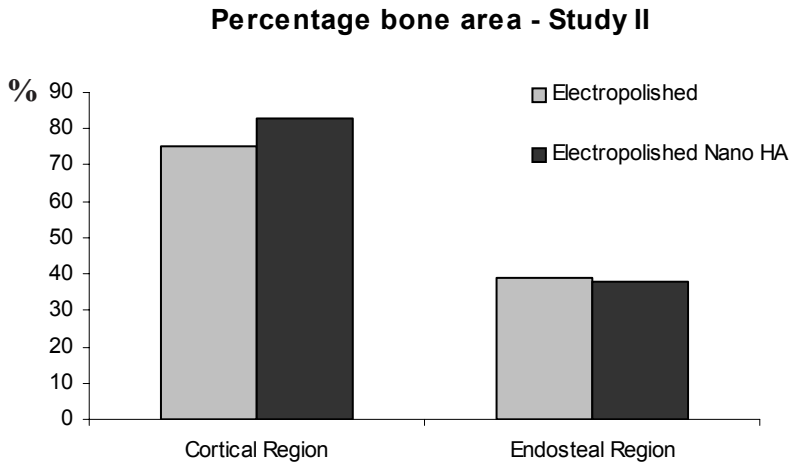

Figure 9 B. The percentage of bone area in study II.

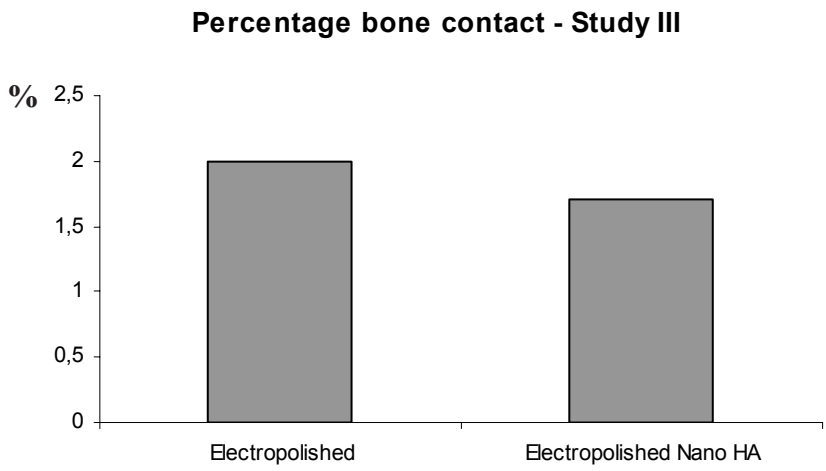

Figure 10 A. The percentage of bone contact in study III.

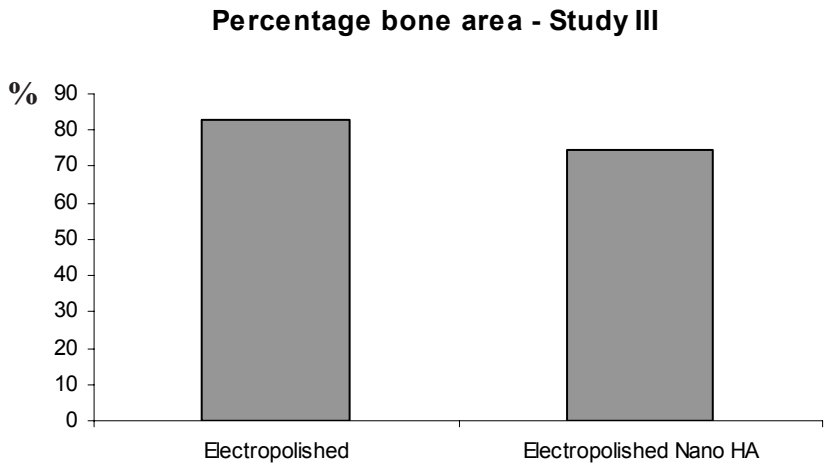

Figure 10 B. The percentage of bone area inside the gap in study III.

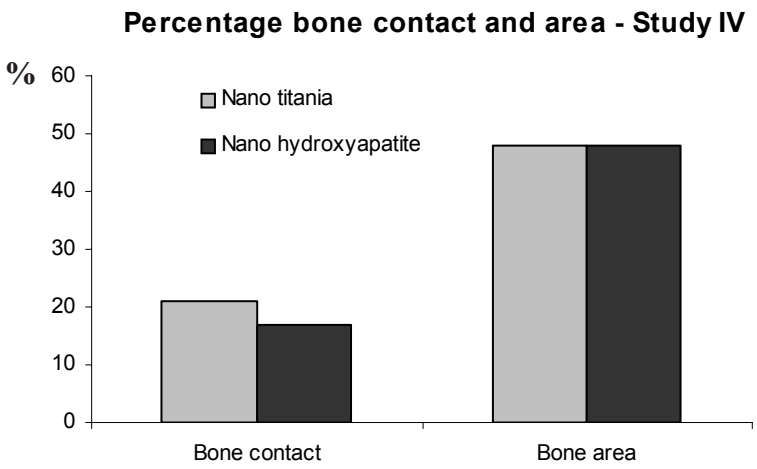

Figure 11. The percentage of bone contact and area in study IV.

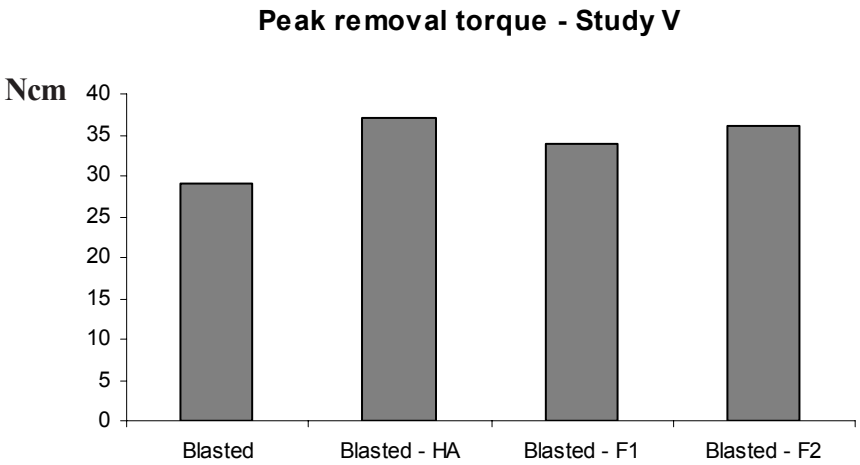

Figure 12 . A diagram showing the removal torque values in study V.

Discussion of methods

Study Design

Implant design

Oral implants currently in use are based on the screw-shaped designs initially introduced by Brånemark et al[1], which provides macro-retention immediately after implant installation. The choice of an experimental cylindrical design, with a very smooth surface, is related to the general aim of the present thesis. Cylindrical smooth implants used do not exhibit macro-threads or surface microstructures. Hence, the variables that affect early bone formation are reduced. Furthermore, nano size features applied with controlled dimensions on this experimental model ensured that: *the bone formation observed to the implant surface was dependent on the created nanotopography*. Moreover, cylindrical implants provide a favorable design for surface topography evaluation at higher resolution with AFM.
The experimental model used in the study I-IV is not suitable for clinical applications. In study V, a blasted screw shaped implant was selected. This implant design corresponds to current available oral implants.

Stabilization plate (Study I-IV)

To verify the fixation of the complex - cylindrical implant and stabilization plate - a test was carried out in a universal testing machine (DL-10000, Emic, Parana , Brazil). The test was performed with a load cell of 50 kgF and speed of 1 mm/min. The actuator was positioned on the top of the implant (test) and on the square part of the stabilization plate (control) to investigate potential displacement of the implant in relation to the plate (Fig. 13). Seven tests were performed for each group and no difference in displacement was detected between the test and control groups.
A representative graph of the implant and plate displacement with increasing load is shown in Figure 14. *Thus, the stabilization plate ensured adequate fixation of the implant, despite the lack of macro and micro retention at the surface*. Additionally, the stabilization plate provides the *same fixation no matter the implant surface properties* and bone response is not affected by potential differences of initial stability.

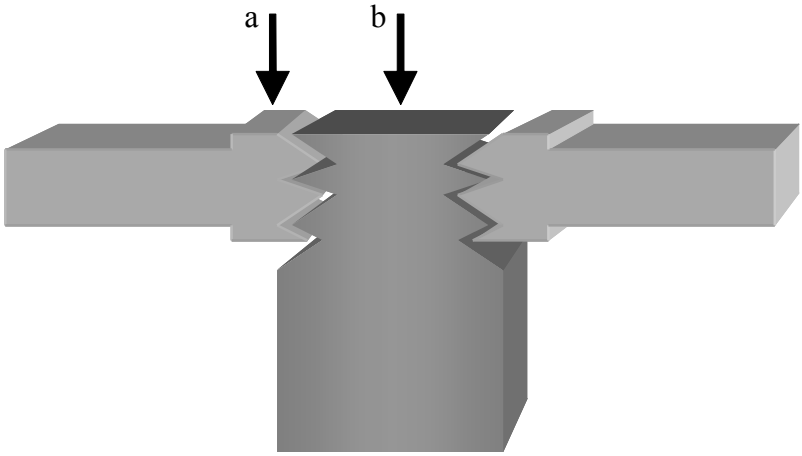

Figure 13. The arrow (a) shows the actuator position on the square part of the stabilization plate (control). The arrow (b) shows the actuator position on the tested implant.

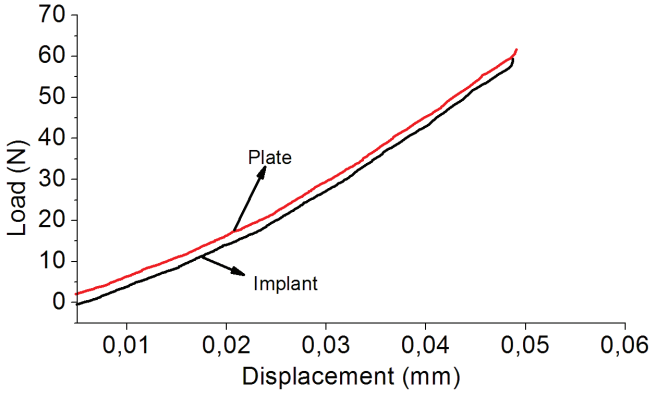

Figure 14. Identical lines curve showing the displacement X load of the implant and of the stabilization plate. There is an offset on the y axis of + 5% of the plate line curve in order to distinguish it from the implant line curve to avoid overlap.

Topographical analysis

Using two resolution levels – AFM/Interferometer

The choice to use two equipments for surface topographical characterization is explained by the difference in resolution of the interferometer and the AFM equipments; and by the need to characterize structures at these two levels of resolution.
The cylindrical implants investigated in the study II-IV were polished to remove the microstrucutres and further coated with nano size features. The interferometer evaluation was performed to: (1) verify the absence of microstructures on the polished surfaces and (2) investigate the final nano coated surface, i.e. whether the coating procedure altered the implant surface at the micro level. AFM evaluation of the cylindrical implants (Study II-IV) was performed to characterize the applied nano structures that varied from 10 nm to 250 nm in diameter. Such small structures would not be detected by the interferometer.
In study V, the implant surface was numerically evaluated only with interferometer. AFM equipment has a limited vertical range of 6 μm that is unsuitable to evaluate moderately rough screw-shaped implants. The nano size features morphology was evaluated by SEM in study V.

Filter selection

Interferometer measurements (200x260μm) were further processed with a Gaussian high pass filter with a size of 50x50 μm to separate form, waviness and roughness. Gaussian filters are indicated to remove form and waviness from measurements of surfaces with rich features. The ideal filter size and measurements area has been investigated by Wennerberg[36] and the values recommended have been used in the present thesis.
AFM measurements (10x10μm) exhibited steps between subsequent scan lines. A polynomial plane correction that levels each scan line was selected. The LMS fit method substracts a fitted polynomial function from each individual scan line with a polynomial degree defined by the user. Polynomial degrees may be set between 0 and 5. Degrees greater than 3 are seldom recommended because the fit might then start to match the real surface structure more than the undesired plane error[130]. In order to investigate the ideal polynomial degree for the AFM measurements, the 1st, 2nd and 3rd polynomial degree was tested on study IV. The surface roughness parameters, the subtracted image and the processed image were evaluated and the results are shown in Figure 15 and Table 5.

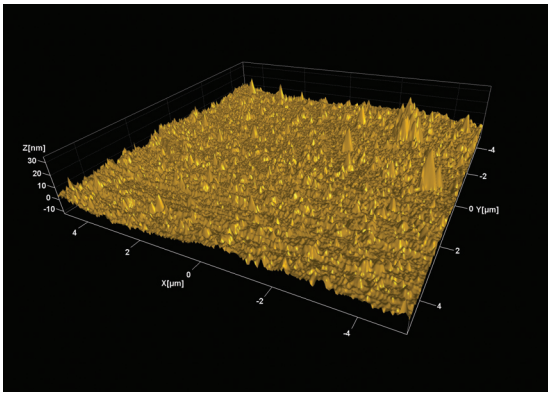

Figure 15 A. The original nano HA coated implant AFM measurement (10x10 µm). The observed form, waviness and the steps between the scan lines should be removed before surface roughness evaluation and nano structures characterization.

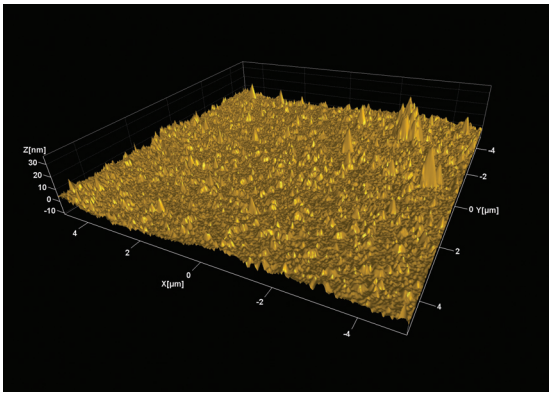

Figure 15 B1. Measurement after correction with the 1st degree of the LMS fit method.

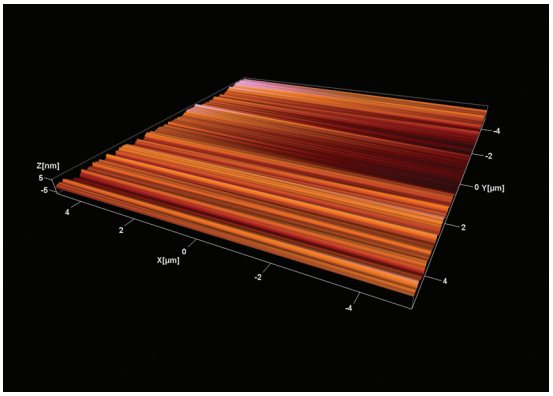

Figure 15 B2. What was removed from the original measurement after correction with the 1st degree of the LMS fit method.

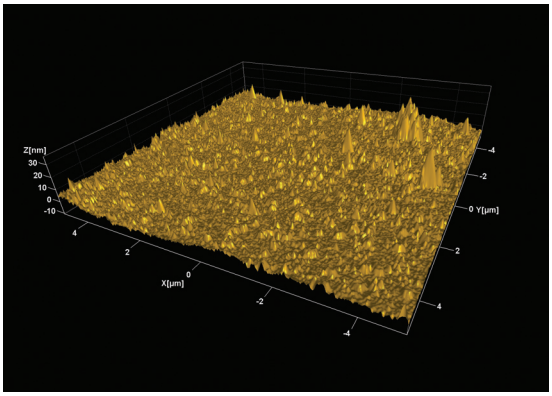

Figure 15 C1. Measurement after correction with the 2nd degree of the LMS fit method.

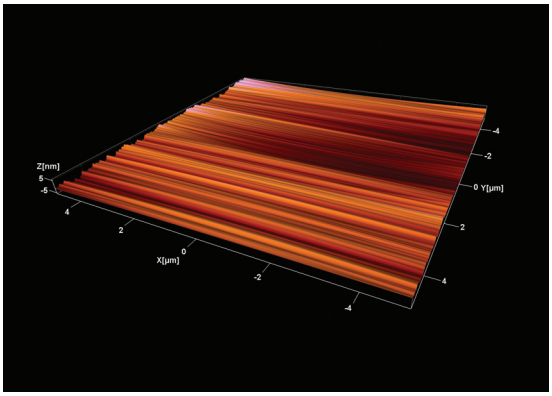

Figure 15 C2. What was removed from the original measurement after correction with the 2nd degree of the LMS fit method.

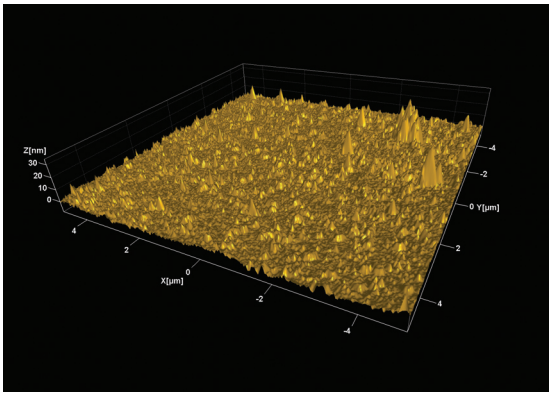

Figure 15 D1. Measurement after correction with the 3rd degree of the LMS fit method.

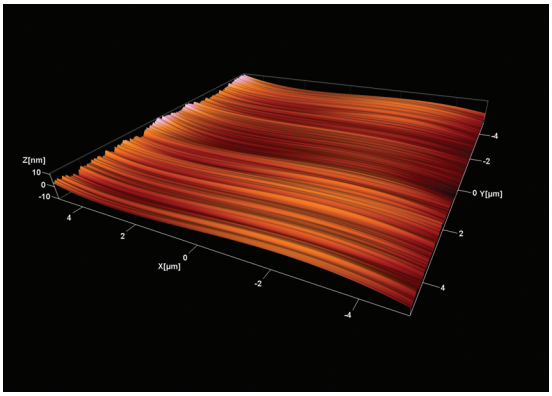

Figure 15 D2. What was removed from the original measurement after correction with the 3rd degree of the LMS fit method.

Table 5 The influence of the least mean square polynomial degree (1-3) on surface roughness of nano coated titania (T) and hydroxyapatite implants (HA) from study IV. AFM area measurements of 10x10 µm measured on the bottom, middle and top part of three implants of each group. S_a (nm), S_{ds} (μm^{-2}) and S_{dr} (%).

	1st			2nd			3rd		
	S_a	**S_{ds}**	**S_{dr}**	**S_a**	**S_{ds}**	**S_{dr}**	**S_a**	**S_{ds}**	**S_{dr}**
T1_1	13	24	0.19	4.8	24	0.16	4.2	24	0.15
T1_2	7.7	25	0.12	4.5	25	0.11	4.3	25	0.11
T1_3	30	12	0.57	17	20	0.58	16	20	0.58
T2_1	9.8	21	0.09	5	22	0.08	4.4	23	0.08
T2_2	43	11	0.57	31	12	0.64	28	13	0.87
T2_3	21	16	0.23	19	18	0.24	13	18	0.21
T3_1	9.8	15	0.12	6.9	16	0.1	5.3	19	0.1
T3_2	10	14	0.18	7.9	15	0.17	7.4	16	0.19
T3_3	11	17	0.22	7.3	18	0.19	5.6	19	0.18
Mean	**17.26**	**17.22**	**0.25**	**11.49**	**18.89**	**0.25**	**9.80**	**19.67**	**0.27**
SD	12.00	5.04	0.19	9.05	4.28	0.21	8.02	3.87	0.27
HA1_1	48	14	4.4	36	14	4	28	14	3.6
HA1_2	28	16	1.8	20	16	1.7	17	17	1.6
HA1_3	40	16	4	29	16	3.5	25	16	3.3
HA2_1	19	19	1.4	17	20	1.5	13	21	1.4
HA2_2	47	16	4.2	34	17	3.8	23	17	3.6
HA2_3	27	17	2.9	20	17	2.8	17	17	2.7
HA3_1	105	20	6.2	45	19	3.9	32	19	3.5
HA3_2	36	17	4	29	18	3.9	27	18	4.6
HA3_3	30	25	3.5	23	25	3.3	15	25	3.3
Mean	**42.22**	**17.78**	**3.58**	**28.11**	**18.00**	**3.16**	**21.89**	**18.22**	**3.07**
SD	25.41	3.23	1.44	9.12	3.16	0.96	6.62	3.19	1.02

3D Topographical Parameters

Surfaces are naturally based on a 3D scale. 2D surface characterization represents only part of the structures present at the surface, and conclusive assumptions of the surface topography with a 2D profiling characterization, should be avoided. Dong et al[133] discussed the importance of describing numerically a surface with the roughness parameters based on a 3D analysis. 3D analysis exhibits advantages compared to 2D analysis: 1. surface topography is three dimensional in nature; 2. the parameters obtained are more realistic, specially the extreme parameters; 3. new parameters can be described, such as S_{ci} (surface fluid core index), recently reported as relevant for osseointegration[134]; 4. larger volume of data is obtained, providing more reliable and representative analysis and; 5. allows proper visualization of the surface[133]. The S parameters, described by Stout[131], are standard parameters of 3D evaluations. In the present thesis, all surface roughness measurements were based on 3D analyses and one *amplitude*-average height deviation (S_a); one *hybrid*-surface developed ratio (S_{dr}) and one *spatial* – density of summits (S_{ds}) parameters were calculated to described surface roughness of each measurement.

Detection of Nano structures

Each individual structure detected at the surface does not represent solely the particle dimensions exhibited in the solution where the implant was dipped. Furthermore, the applied particle sizes may be modulated by different factors during its synthesis and may vary depending on the coating technique parameters used. *Thus, the nano structures detected at the implant surface represent a combination of the pre-existing topography combined with those achieved by the synthesis-coating technique.* In Figure 16, some potential combination of the pre-existing structures and the applied structures is shown. Numerous reports of nano based materials failed to show nano structures at the surface with size equivalent to the one present in the precursor material, which could be a powder or a solution. This is usually caused by particle agglomeration that may end up with micro-sized structures. Another relevant issue in the detection process is to distinguish the applied structures from the pre-existing structures. Simply calculating the mean value and claiming that the difference corresponds to the "new" structures is not ideal. In the present thesis, not only the difference in mean values was reported; a frequency histogram showed the range of each feature size segment existent before and after the coating. *Thus, it was possible to verify the dimensions of the applied nano features at the implant surface.* The different range of sizes of the structures may also be visualized at the surface, adding more data of the nano modified surface.

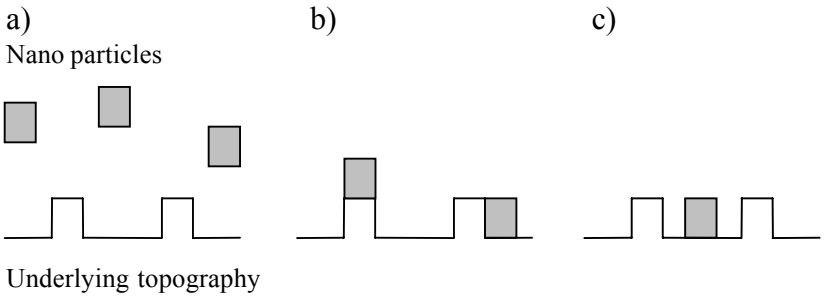

Figure 16.Schematic illustration of some potential combinations of the underlying topography, with pre-existing structures, together with the particles present in the solution (a). The modified surface may exhibit higher or wider features (b); or may also exhibit increased feature density (c).

Bone Response Evaluation Methods

Histomorphometric Evaluation

The amount of titanium and the very smooth implant surface did not allow further grinding to a 10 µm thick section, following the preparation technique described by Donath[132]. Initial attempts to reach the ideal 10 µm thick section resulted in implant de-attachment and damage to the surrounding tissues. A thickness of 40 µm was found safe for the sections in study I-IV. Johansson & Morberg[135] reported that section with this thickness may produce overestimated bone contact values. No difference in bone area can be expected comparing sections in the range of 10-40 µm thickness. Bone-implant contact and bone area measurements have been used in numerous doctoral projects at the Biomaterials Department and is a standard technique to evaluate bone-implant interface.
The threshold Red-Blue-Green *3 steps* technique for histomorphometry measurement represents a very fast and reliable method to calculate bone area and bone contact values. The threshold RGB tool is especially valuable to measure implants with complex shape (Fig. 17).

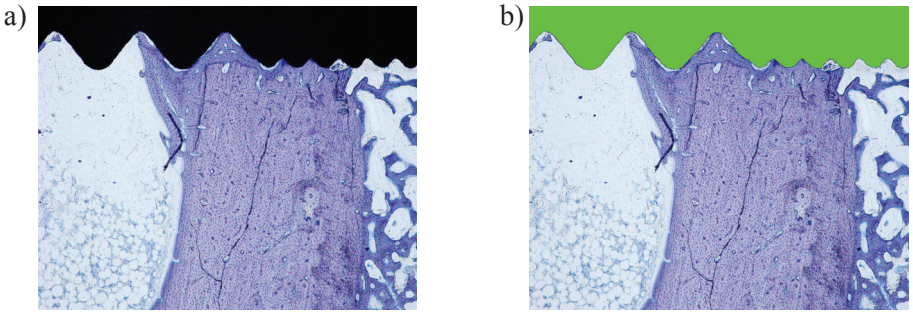

Figure 17. Screw shaped implants (a) used in study V. The macro and micro threads are marked automatically (b), despite the complex design.

Removal torque test

The removal torque test has been used routinely for evaluation of screw-shaped implant with surface topography at the micro level and have been reported to be correlated with the bone implant contact values[4,136]. However, nano size modified implants have not been evaluated before and the reliability (repeatability) of the method should be investigated for this purpose. The removal torque reliability test was performed in study V. The values of the two identical fluoride-modified surfaces were very similar, which supports reliability of the removal torque method. *The removal torque test is a reliable method for evaluation of bone response to implants modified with nano size structures.*

Discussion of results

Rationale behind each study

Study I – *Validate the model*

Micro structures and macro threads are known to affect bone response. An experimental model to evaluate solely the effect of nano size structures must be free of micro structures (very smooth surfaces) and free of macro threads (cylindrical). The smooth cylindrical implant should have a device to ensure adequate stability, avoiding micro movements known to affect bone formation. A stabilization plate was implemented to ensure adequate fixation of the smooth cylindrical implant during the experiments. The model was tested in Study I and proved to be suitable to evaluate implants modified with nano size structures, as observed in Studies II-IV.

Study II – *Effect of nano size HA structures*

The effect of nano HA structures added on smooth cylindrical implants on bone response was investigated. The detection of nano size structures was performed on AFM measurements combined with image processor software. *Firstly*, the nano HA coating method produced nano size structures at the implant surface with equivalent size of the particles present in the precursor solution (where the nano HA particles are synthesized). *Secondly,* the added nano HA structures to smooth cylindrical implants enhanced bone formation. However, the enhanced bone formation could be an effect of the nano HA chemistry or the nano topography; or a synergetic effect of both chemistry and nano topography.

Study III – *Effect of nano size HA structures placed in a gap*

The results from Study II showed that nano HA structures enhanced bone formation in a model without gap. The potential effect of nano HA on a gap healing design was investigated in study III. Therefore, nano HA modified implants were compared to electropolished implants placed in a gap. Control uncoated and nano HA coated implants exhibited similar roughness and porosity parameters on AFM measurements. After 4 weeks of healing, similar bone response was observed to both control and nano HA coated implants. This result indicates that bioactivity of nano HA was not supported in this gap healing model.

Study IV – *Effect of "bioinert" and "bioactive" surfaces*

In this last study with the experimental smooth cylindrical implants, a direct approach was selected in order to separately investigate the effect of surface chemistry and the effect of nano size structures added to the implant surface. Here, both control and test implants had been coated with nano size structures. The control implants were coated with "bioinert" nano titania structures whereas test implants were coated with "bioactive" nano HA structures, i.e.

the aim was to investigate whether nano HA structures would result in enhanced osseointegration compared to nano titania structures. The bone response to nano titania coated implants was 24% higher compared to nano HA coated implants, although the difference was not significant. The present study did not support the enhanced bone formation to hydroxyapatite compared to titania materials.

Study V – *Nano size structures for oral implants*

The findings from the previous studies with very smooth implants showed that: the presence of nano size structures with specific dimensions at the implant surface enhances bone response, irrespective of the surface chemistry. The enhanced bone response to nano size structures could only occur to very smooth experimental implants. In study V, the hypothesis of enhanced bone response to moderately rough screw shaped implants modified with implemented nano size structures was investigated. Fluoride-modified and nano HA coated implants that possess nano size structures, showed a tendency of enhanced bone response (17-25%) compared to control implants, without similar nano size structures.

Surface Roughness and Chemistry

The surface roughness values from the implants prepared with the same method exhibited similar values as measured on the top, middle and bottom part of the implants. This was shown in detail in study II. Statistical analyses revealed similar surface roughness values evaluated on the top, middle and bottom part for both electropolished and modified electropolished surfaces with nano HA. Different surface roughness along the implant could affect bone formation, especially in the rabbit tibia model, where the rabbit cortex is in the same region as the top part of the implant.

The apparent contradictory results of increased roughness in Study II and decreased roughness in Study V, observed with the nano HA modification, is explained by the different underlying topography. In study II, the implants were electropolished to produce a very smooth surface; by contrast, the underlying topography in Study V was moderately rough. Thus, the applied nano crystals introduced structures on the very smooth implants (study II), increasing surface roughness; whereas in the moderately rough implants (study V), the nano crystals reduced the depth of the valleys and broadened the peaks, decreasing slightly the surface roughness. The etching with diluted HF acid produced a similar effect. The edges of the microstructures were smoothened and on the microstructured walls, nanostructures produced by the acid etching could be detected.

The decrease in surface roughness to "rougher" surfaces could already be observed in Study IV, where the underlying topography evaluated by interferometer exhibited a S_a of 225 nm. Mechanically polished surfaces to be modified with nano -HA and -titania, were rougher compared to the electropolished implants from Study II (S_a = 94 nm) and Study III (S_a = 49

nm), and exhibited increased surface roughness values compared to the final surfaces in Study IV modified with nano HA (S_a = 170 nm) and titania (S_a = 121 nm).

The difference of the surface roughness values from the underlying topography (control) and the modified implants was, in all the studies, within the nanometer range; and alone could not explain the bone response observed in the present studies. In study IV, nano titania implants exhibited decreased S_a values, both on interferometer and AFM measurements, for the nano titania compared to nano HA implants. However, the bone response was 24% higher for the nano titania compared to the nano HA implants. In study V, the implementation of nano structures through coating with nano HA particles and etching with diluted hydrofluoric acid showed a tendency of increased bone formation compared to control (blasted) implants. The topography evaluation performed with the interferometer demonstrated decreased surface roughness at the nanometer range for the nano HA coated and for the fluoride-modified implants compared to the blasted implant, which represented the underlying surface. Removal torque values were lower for the rougher blasted implant compared to the smoother blasted nano HA and smoothest blasted fluoride-modified implants. *The present results do not support the modulation of bone response by differences of surface roughness values on the nanometer range alone.*

The surface modifications used in the present thesis revealed differences in chemical composition and nanotopography of the implant surface. The mechanisms that may explain the enhanced bone formation found in the present thesis to nano size structures with specific dimensions at the implant surface are not fully understood. At this moment, is not possible to affirm that bone tissue response is modulated only by surface chemistry or topography, or more probably by a synergetic effect of both variables.

The bioactive materials described by Osborn & Newesely[28] showed direct bonding between the implant and adjacent bone. One of the precursor materials to be classified as bioactive was hydroxyapatite. In the present thesis, nano HA modification lead to increased bone formation in studies II and V when compared to control implants that lack of applied nano structures. However, in study IV, when a direct approach compared the "bioactive" HA to "bioinert" titania, the bone response observed was the opposite as could be expected. Although not statistically significant, increase of 24% of bone contact was found to the "bioinert" (titania) compared to "bioactive" (HA) materials. Moreover, nano HA implants, evaluated in study V, showed similar removal torque compared to fluoride-modified implants with reduced amount of fluoride at the surface. Some parameters of the nano size structures described in the present thesis are not part of routine surface analyses of osseointegrated implants and it was demonstrated to be relevant for bone tissue formation. Thus, *the surface chemistry effect of HA alone may not explain the enhanced early bone formation in the present studies.*

The need of a specific micro- and nano- topography was showed clearly in study III. Very smooth implants with similar nano structure dimensions failed to show differences in bone formation, despite the presence of nano HA in a gap healing model. Thus, the enhanced bone response to bioactive materials can be explained by specific structures added to the surface

during the chemical treatment. If there is a beneficial effect of the surface chemistry it will occur in the presence of a specific topography.

Surface features

In the present thesis, the surface modifications investigated produced nano size structures at the surface with specific dimensions. In study II, the nano HA modification increased surface feature diameter in 6 nm, equivalent to the particles present in the solution. In addition, nano HA implants showed increased surface porosity and number of pores on the nano level of resolution; that may act as binding sites for the biomolecules involved in the early healing phase, which could explain the enhanced bone formation. In study III, surface porosity was similar between the electropolished and electropolished + nano HA implants. Moreover, the differences in pore diameter and number of pores were not as remarkable as observed in study II. Despite the different surface chemistry composition of the electropolished and modified electropolished surfaces with nano HA, the bone formation in the gap healing model observed in study III was similar. In study IV, the features detected at the nano HA implant had a discrete higher diameter compared to the nano titania. Increased feature height was also observed for the nano HA, whereas the surface coverage area was almost 2 times higher for the nano titania with a remarkable increase in the surface feature density. The bone response was 24% higher for the nano titania compared to the nano HA, although not statistically significant. The present results revealed that applied nano structures with different dimensions enhanced bone formation, independent of the surface chemical composition. *The present results showed enhanced bone formation to titanium implants modified with nano size structures with specific dimensions.*

The ideal feature dimensions and distribution for enhanced bone response require more experiments. Moreover, the surface properties of an implant with nano size structures will differ from those with micro size structures, with respect to dissolution. A recent experiment reported higher ionic dissolution rate to nano HA based materials compared to conventional HA materials[137]. Thus, more ions were released at the interface of nano sized materials that may modulate cell activity and tissue formation. The increased availability of ions at the interface is also applicable for the fluoride-modified implants with nano size structures or any material that possess nano size structures, as discussed by Hench[138]. More recently, sub-nanometer structure morphology of nano HA particles has been characterized by TEM[139] and may also influence early healing events at the interface.

The present thesis and future perspectives of it can be summarized as follows:
In the absence of micro structures, the present thesis, presumably for the first time in vivo, evidenced enhanced early bone response from varying the nano structures alone. Moreover, a 17-25% enhanced bone response to nano structures was demonstrated on moderately rough surfaces too, although this difference was not significant. The presence of nano-size structures, irrespective of varying surface chemistry (fluoride, HA or titania), resulted in evidence of supported bone formation. The next focus will be on the "ideal" nano structure dimension and distribution at the implant surface that is coupled to an enhanced bone response. It is possible to produce different nano structures by varying some parameters of the surface modifications used in the present thesis. By varying the nano structure dimension and distribution it may be possible to increase the knowledge of osseointegration mechanisms and modulate the bone response. Bone healing to osseointegrated implants follows a sequence of events that is time dependent. This factor adds an extra challenge to the design of an "optimal" surface for osseointegrated implants. The surface must function properly from the early hours of the inflammatory response up to several years and withstand dynamic loading; indeed implant surfaces must meet the demands from a biomolecule viewpoint and enable proper stress transfer at the bone-implant interface. Future experiments must evaluate the clinical long-term results of the "add-on" coatings used in the present thesis and ensure the integrity of the bone-implant interface that will determine the success of the rehabilitation.

Conclusions

1. A model for evaluation of bone healing to smooth cylindrical titanium implants has been validated and found suitable for further studies

2. Nano size hydroxyapatite structures enhanced early bone formation to smooth titanium implants

3. Nano size hydroxyapatite structures did not affect early bone formation in a gap healing design to smooth titanium implants

4. Smooth titanium implants modified with nano size "bioinert" or "bioactive" surfaces showed similar bone formation

5. Moderately rough screw shaped implants with nano size structures of different chemical compositions showed a tendency of enhanced bone formation compared to blasted controls without added nano structures

Acknowledgements

I would like to thank everyone involved in this work for their support and for making my thesis possible. I wish to express my special thanks to:

Ann Wennerberg for outstanding and reliable guidance, for her sharp eyes in all hypotheses to put the work always on the right track, and never failing support and enthusiasm throughout these years, and for giving me freedom to carry out this project.

Tomas Albrektsson for inspiration, constructive criticism and for sharing a rare knowledge of the field with wise words and great discussions. Special thanks for the warm support to my family.

Magnus Jacobsson and Lars Sennerby, for great collaboration and discussions.

Altair Cury and Carlos Elias for all your interest and continuous support over the years.

Carina Johansson and Peter Thomsen for inspiring discussions about research and others interesting subjects.

Stig Karlsson for welcoming me at the Dept Prosthodontics and for introducing me to Ann Wennerberg

Gunnar E. Carlsson for having a great interest in my work, always a smile and friendly chats.

Anna Arvidsson, Anna Göransson and Victoria Franke Stenport for helping me in the early days with all the equipments and valuable contribution.

Gunilla Aronsson, Maria Hoffman and Petra Johansson for all their support, excellent work and for always being helpful.

My co-authors Fredrik Currie, Ilkka Kangasniemi, Per Kjellin, Lory Melin, Martin Andersson and Timo Peltola for stimulating collaborations.

Stefan Rosen and Karin Westerberg at Toponova and Image Metrology staff for generous technical support.

Barbro Lanner, Katarina Nobelius and Nina Klubal for kindly helping with administrative matters.

All colleagues at the Departments of Prosthodontics and Biomaterials for friendly support during these years and all good moments.

Finally, my wife Cristiane, my parents Maria and Luiz, my sister Ana and my brother Andre for love, support and for always being there.

This work was supported by grants from CAPES, Research Agency from the Brazilian Ministry of Education and Hjalmar Svensson Research Foundation.

References

1. Branemark PI, Adell R, Breine U, Hansson BO, Lindstrom J, Ohlsson A. Intra-osseous anchorage of dental prostheses. I. Experimental studies. Scand J Plast Reconstr Surg 1969;3(2):81-100.
2. Branemark PI, Hansson BO, Adell R, Breine U, Lindstrom J, Hallen O, Ohman A. Osseointegrated implants in the treatment of the edentulous jaw. Experience from a 10-year period. Scand J Plast Reconstr Surg Suppl 1977;16:1-132.
3. Albrektsson T, Dahl E, Enbom L, Engevall S, Engquist B, Eriksson AR, Feldmann G, Freiberg N, Glantz PO, Kjellman O and others. Osseointegrated oral implants. A Swedish multicenter study of 8139 consecutively inserted Nobelpharma implants. J Periodontol 1988;59(5):287-96.
4. Johansson C. On tissue reactions to metal implants. Göteborg: Göteborg University; 1991.
5. Carlsson L. On the development of a new concept for orthopaedic implant fixation [PhD]. Göteborg: Göteborg University; 1989.
6. Sennerby L. On the bone tissue response to titanium implants. Göteborg: Göteborg University; 1991.
7. Naert I, Koutsikakis G, Duyck J, Quirynen M, Jacobs R, van Steenberghe D. Biologic outcome of single-implant restorations as tooth replacements: a long-term follow-up study. Clin Implant Dent Relat Res 2000;2(4):209-18.
8. van Steenberghe D, Lekholm U, Bolender C, Folmer T, Henry P, Herrmann I, Higuchi K, Laney W, Linden U, Astrand P. Applicability of osseointegrated oral implants in the rehabilitation of partial edentulism: a prospective multicenter study on 558 fixtures. Int J Oral Maxillofac Implants 1990;5(3):272-81.
9. Junqueira L, Carneiro J. Histologia Básica. Rio de Janeiro: Guanabara Koogan; 1995.
10. Buckwalter JA, Glimcher MJ, Cooper RR, Recker R. Bone biology. I: Structure, blood supply, cells, matrix, and mineralization. Instr Course Lect 1996;45:371-86.
11. Bilezikian J, Raisz L, Rodan G. Principles of bone biology. San Diego: Academic Press; 2002.
12. Aubin JE. Bone stem cells. J Cell Biochem Suppl 1998;30-31:73-82.
13. Muenzenberg KJ, Gebhardt M. Brushite octacalcium phosphate, and carbonate-containing apatite in bone. Clin Orthop Relat Res 1973(90):271-3.
14. Anderson HC. Molecular biology of matrix vesicles. Clin Orthop Relat Res 1995(314):266-80.
15. Traub W, Arad T, Weiner S. 3-Dimensional Ordered Distribution of Crystals in Turkey Tendon Collagen-Fibers. Proceedings of the National Academy of Sciences of the United States of America 1989;86(24):9822-9826.

16. Robinson RA, Watson ML. Collagen-crystal relationships in bone as seen in the electron microscope. Anat Rec 1952;114(3):383-409.
17. Mc CD. The crystal chemistry of carbonate apatities and their relationship to the composition of calcified tissues. J Dent Res 1952;31(1):53-63.
18. LeGeros RZ. Calcium phosphates in oral biology and medicine. Monogr Oral Sci 1991;15:1-201.
19. Pellegrino ED, Biltz RM. Mineralization in the chick embryo. I. Monohydrogen phosphate and carbonate relationships during maturation of the bone crystal complex. Calcif Tissue Res 1972;10(2):128-35.
20. Rey C, Renugopalakrishnan V, Collins B, Glimcher MJ. Fourier transform infrared spectroscopic study of the carbonate ions in bone mineral during aging. Calcif Tissue Int 1991;49(4):251-8.
21. LeGeros RZ. Properties of osteoconductive biomaterials: calcium phosphates. Clin Orthop Relat Res 2002(395):81-98.
22. Miller A. Collagen: the organic matrix of bone. Philos Trans R Soc Lond B Biol Sci 1984;304(1121):455-77.
23. Weiner S, Price PA. Disaggregation of bone into crystals. Calcif Tissue Int 1986;39(6):365-75.
24. Wachtel E, Weiner S. Small-angle x-ray scattering study of dispersed crystals from bone and tendon. J Bone Miner Res 1994;9(10):1651-5.
25. Aumailley M, Gayraud B. Structure and biological activity of the extracellular matrix. J Mol Med 1998;76(3-4):253-65.
26. Adams JC. Cell-matrix contact structures. Cell Mol Life Sci 2001;58(3):371-92.
27. Albrektsson T, Branemark PI, Hansson HA, Lindstrom J. Osseointegrated titanium implants. Requirements for ensuring a long-lasting, direct bone-to-implant anchorage in man. Acta Orthop Scand 1981;52(2):155-70.
28. Osborn JF, Newesely H. Dynamic aspects of the implant-bone-interface. In: Heimke G, editor. Dental implant: Materials and systems; 1979; Munchen. Hanser. p 111-123. (Dental implant: Materials and systems).
29. Hazan R, Brener R, Oron U. Bone growth to metal implants is regulated by their surface chemical properties. Biomaterials 1993;14(8):570-4.
30. Kanagaraja S, Wennerberg A, Eriksson C, Nygren H. Cellular reactions and bone apposition to titanium surfaces with different surface roughness and oxide thickness cleaned by oxidation. Biomaterials 2001;22(13):1809-18.
31. Kim HM, Miyaji F, Kokubo T, Nakamura T. Preparation of bioactive Ti and its alloys via simple chemical surface treatment. J Biomed Mater Res 1996;32(3):409-17.
32. Kim HM, Miyaji F, Kokubo T, Nakamura T. Bonding strength of bonelike apatite layer to Ti metal substrate. J Biomed Mater Res 1997;38(2):121-7.

33. Nishiguchi S, Fujibayashi S, Kim HM, Kokubo T, Nakamura T. Biology of alkali- and heat-treated titanium implants. J Biomed Mater Res A 2003;67(1):26-35.
34. Nishiguchi S, Kato H, Fujita H, Oka M, Kim HM, Kokubo T, Nakamura T. Titanium metals form direct bonding to bone after alkali and heat treatments. Biomaterials 2001;22(18):2525-33.
35. Nishiguchi S, Kato H, Neo M, Oka M, Kim HM, Kokubo T, Nakamura T. Alkali- and heat-treated porous titanium for orthopedic implants. J Biomed Mater Res 2001;54(2):198-208.
36. Wennerberg A. On surface roughness and implant incorporation [PhD]. Göteborg: Göteborg University; 1996.
37. Engquist B, Astrand P, Dahlgren S, Engquist E, Feldmann H, Grondahl K. Marginal bone reaction to oral implants: a prospective comparative study of Astra Tech and Branemark System implants. Clin Oral Implants Res 2002;13(1):30-7.
38. van Steenberghe D, De Mars G, Quirynen M, Jacobs R, Naert I. A prospective split-mouth comparative study of two screw-shaped self-tapping pure titanium implant systems. Clin Oral Implants Res 2000;11(3):202-9.
39. Lausmaa J. Mechanical, Thermal, Chemical and Electrochemical surface treatment of titanium. In: Brunette DM, Tengvall P, Textor M, Thomsen P, editors. Titanium in medicine: materials science, surface science, engineeiring, biological responses and medical applications. Berlin: Springer; 2001.
40. Masaki C, Schneider GB, Zaharias R, Seabold D, Stanford C. Effects of implant surface microtopography on osteoblast gene expression. Clin Oral Implants Res 2005;16(6):650-6.
41. Cooper LF, Zhou Y, Takebe J, Guo J, Abron A, Holmen A, Ellingsen JE. Fluoride modification effects on osteoblast behavior and bone formation at TiO2 grit-blasted c.p. titanium endosseous implants. Biomaterials 2006;27(6):926-36.
42. Isa ZM, Schneider GB, Zaharias R, Seabold D, Stanford CM. Effects of fluoride-modified titanium surfaces on osteoblast proliferation and gene expression. Int J Oral Maxillofac Implants 2006;21(2):203-11.
43. Ellingsen JE. Pre-treatment of titanium implants with fluoride improves their retention in bone. J Mater Sci: Mater Med 1995;6:749-753.
44. Ellingsen JE, Johansson CB, Wennerberg A, Holmen A. Improved retention and bone-tolmplant contact with fluoride-modified titanium implants. Int J Oral Maxillofac Implants 2004;19(5):659-66.
45. Jarcho M. Calcium phosphate ceramics as hard tissue prosthetics. Clin Orthop Relat Res 1981(157):259-78.
46. Jarcho M, Kay JF, Gumaer KI, Doremus RH, Drobeck HP. Tissue, cellular and subcellular events at a bone-ceramic hydroxylapatite interface. J Bioeng 1977;1(2):79-92.

47. Ducheyne P, Qiu Q. Bioactive ceramics: the effect of surface reactivity on bone formation and bone cell function. Biomaterials 1999;20(23-24):2287-303.
48. Ducheyne P, Cuckler JM. Bioactive ceramic prosthetic coatings. Clin Orthop Relat Res 1992(276):102-14.
49. Brown WE, Eidelman N, Tomazic B. Octacalcium phosphate as a precursor in biomineral formation. Adv Dent Res 1987;1(2):306-13.
50. Bagambisa FB, Joos U, Schilli W. Mechanisms and structure of the bond between bone and hydroxyapatite ceramics. J Biomed Mater Res 1993;27(8):1047-55.
51. Ogiso M, Tabata T, Ichijo T, Borgese D. Examination of human bone surrounded by a dense hydroxyapatite dental implant after long-term use. J Long Term Eff Med Implants 1992;2(4):235-47.
52. Ogiso M, Yamashita Y, Matsumoto T. Microstructural changes in bone of HA-coated implants. J Biomed Mater Res 1998;39(1):23-31.
53. Chin KOA, Nancollas GH. Dissolution of Fluorapatite - a Constant-Composition Kinetics Study. Langmuir 1991;7(10):2175-2179.
54. Nelson DG, Featherstone JD, Duncan JF, Cutress TW. Effect of carbonate and fluoride on the dissolution behaviour of synthetic apatites. Caries Res 1983;17(3):200-11.
55. Nelson DGA, Barry JC, Shields CP, Glena R, Featherstone JDB. Crystal Morphology, Composition, and Dissolution Behavior of Carbonated Apatites Prepared at Controlled Ph and Temperature. Journal of Colloid and Interface Science 1989;130(2):467-479.
56. de Putter C, de Groot K, Sillevis S. Implants of dense hydroxyapatite in prosthetic dentistry. In: Lee A, Albrektsson T, Branemark PI, editors. Clinical aplications of biomaterials. Chichester: John Wiley & Sons; 1982. p 123-31.
57. Kent JN, Quinn JH, Zide MF, Guerra LR, Boyne PJ. Alveolar ridge augmentation using nonresorbable hydroxylapatite with or without autogenous cancellous bone. J Oral Maxillofac Surg 1983;41(10):629-42.
58. Holmes RE, Hagler HK. Porous hydroxyapatite as a bone graft substitute in cranial reconstruction: a histometric study. Plast Reconstr Surg 1988;81(5):662-71.
59. de Putter C, de Groot K, Sillevis Smitt PA. Transmucosal implants of dense hydroxylapatite. J Prosthet Dent 1983;49(1):87-95.
60. Jarcho M. Biomaterial aspects of calcium phosphates. Properties and applications. Dent Clin North Am 1986;30(1):25-47.
61. Cook SD, Thomas KA, Kay JF, Jarcho M. Hydroxyapatite-coated titanium for orthopedic implant applications. Clin Orthop Relat Res 1988(232):225-43.
62. Hayashi K, Uenoyama K, Matsuguchi N, Sugioka Y. Quantitative analysis of in vivo tissue responses to titanium-oxide- and hydroxyapatite-coated titanium alloy. J Biomed Mater Res 1991;25(4):515-23.
63. de Groot K, Geesink R, Klein CP, Serekian P. Plasma sprayed coatings of hydroxylapatite. J Biomed Mater Res 1987;21(12):1375-81.

64. Soballe K. Hydroxyapatite ceramic coating for bone implant fixation. Mechanical and histological studies in dogs. Acta Orthop Scand Suppl 1993;255:1-58.
65. Herman H. Plasma-Sprayed Coatings. Scientific American 1988;259(3):112-117.
66. Ducheyne P, Van Raemdonck W, Heughebaert JC, Heughebaert M. Structural analysis of hydroxyapatite coatings on titanium. Biomaterials 1986;7(2):97-103.
67. Gottlander M, Albrektsson T. Histomorphometric studies of hydroxylapatite-coated and uncoated CP titanium threaded implants in bone. Int J Oral Maxillofac Implants 1991;6(4):399-404.
68. Gottlander M, Albrektsson T, Carlsson LV. A histomorphometric study of unthreaded hydroxyapatite-coated and titanium-coated implants in rabbit bone. Int J Oral Maxillofac Implants 1992;7(4):485-90.
69. Gottlander M, Albrektsson T. Histomorphometric analyses of hydroxyapatite-coated and uncoated titanium implants. The importance of the implant design. Clin Oral Implants Res 1992;3(2):71-6.
70. Gottlander M, Johansson CB, Wennerberg A, Albrektsson T, Radin S, Ducheyne P. Bone tissue reactions to an electrophoretically applied calcium phosphate coating. Biomaterials 1997;18(7):551-7.
71. Rokkum M, Reigstad A, Johansson CB, Albrektsson T. Tissue reactions adjacent to well-fixed hydroxyapatite-coated acetabular cups. Histopathology of ten specimens retrieved at reoperation after 0.3 to 5.8 years. J Bone Joint Surg Br 2003;85(3):440-7.
72. Albrektsson T. Hydroxyapatite-coated implants: a case against their use. J Oral Maxillofac Surg 1998;56(11):1312-26.
73. Bloebaum RD, Beeks D, Dorr LD, Savory CG, DuPont JA, Hofmann AA. Complications with hydroxyapatite particulate separation in total hip arthroplasty. Clin Orthop Relat Res 1994(298):19-26.
74. Bloebaum RD, Zou L, Bachus KN, Shea KG, Hofmann AA, Dunn HK. Analysis of particles in acetabular components from patients with osteolysis. Clin Orthop Relat Res 1997(338):109-18.
75. Ishizawa H, Ogino M. Thin hydroxyapatite layers formed on porous titanium using electrochemical and hydrothermal reaction. Journal of Materials Science 1996;31(23):6279-6284.
76. Ishizawa H, Ogino M. Hydrothermal precipitation of hydroxyapatite on anodic titanium oxide films containing Ca and P. Journal of Materials Science 1999;34(23):5893-5898.
77. Ishizawa H, Fujino M, Ogino M. Mechanical and Histological Investigation of Hydrothermally Treated and Untreated Anodic Titanium-Oxide Films Containing Ca and P. Journal of Biomedical Materials Research 1995;29(11):1459-1468.

78. Giavaresi G, Fini M, Cigada A, Chiesa R, Rondelli G, Rimondini L, Torricelli P, Aldini NN, Giardino R. Mechanical and histomorphometric evaluations of titanium implants with different surface treatments inserted in sheep cortical bone. Biomaterials 2003;24(9):1583-94.
79. Cleries L, Fernandez-Pradas JM, Morenza JL. Bone growth on and resorption of calcium phosphate coatings obtained by pulsed laser deposition (vol 49, pg 43, 2000). Journal of Biomedical Materials Research 2001;57(3):473-473.
80. Peraire C, Arias JL, Bernal D, Leon B, Arano A, Roth W. Biological stability and osteoconductivity in rabbit tibia of pulsed laser deposited hydroxylapatite coatings. Journal of Biomedical Materials Research Part A 2006;77A(2):370-379.
81. de Groot K, Wolke JGC, Jansen JA. Calcium phosphate coatings for medical implants. Proceedings of the Institution of Mechanical Engineers Part H-Journal of Engineering in Medicine 1998;212(H2):137-147.
82. Jansen JA, Wolke JG, Swann S, Van der Waerden JP, de Groot K. Application of magnetron sputtering for producing ceramic coatings on implant materials. Clin Oral Implants Res 1993;4(1):28-34.
83. Mohammadi S, Esposito M, Hall J, Emanuelsson L, Krozer A, Thomsen P. Long-term bone response to titanium implants coated with thin radiofrequent magnetron-sputtered hydroxyapatite in rabbits. Int J Oral Maxillofac Implants 2004;19(4):498-509.
84. Mohammadi S, Esposito M, Hall J, Emanuelsson L, Krozer A, Thomsen P. Short-term bone response to titanium implants coated with thin radiofrequent magnetron-sputtered hydroxyapatite in rabbits. Clin Implant Dent Relat Res 2003;5(4):241-53.
85. Ramires PA, Romito A, Cosentino F, Milella E. The influence of titania/hydroxyapatite composite coatings on in vitro osteoblasts behaviour. Biomaterials 2001;22(12):1467-74.
86. Kim HW, Koh YH, Li LH, Lee S, Kim HE. Hydroxyapatite coating on titanium substrate with titania buffer layer processed by sol-gel method. Biomaterials 2004;25(13):2533-8.
87. Kim HW, Kim HE, Salih V, Knowles JC. Hydroxyapatite and titania sol-gel composite coatings on titanium for hard tissue implants; mechanical and in vitro biological performance. J Biomed Mater Res B Appl Biomater 2005;72(1):1-8.
88. Ebelmen M. Recherches sur les combinaisons des acides borique et silicique avec les éthers. Annales de Chimie et de Physique 1846(16):129-166.
89. Hench LL, West JK. The Sol-Gel Process. Chemical Reviews 1990;90(1):33-72.
90. Li P, de Groot K. Calcium phosphate formation within sol-gel prepared titania in vitro and in vivo. J Biomed Mater Res 1993;27(12):1495-500.
91. Li PJ, Kangasniemi I, Degroot K, Kokubo T. Bonelike Hydroxyapatite Induction by a Gel-Derived Titania on a Titanium Substrate. Journal of the American Ceramic Society 1994;77(5):1307-1312.

92. Bornside DE, Macosko CW, Scriven LE. On the Modeling of Spin Coating. Journal of Imaging Technology 1987;13(4):122-130.
93. Patsi ME, Hautaniemi JA, Rahiala HM, Peltola TO, Kangasniemi IMO. Bonding strengths of titania sol-gel derived coatings on titanium. Journal of Sol-Gel Science and Technology 1998;11(1):55-66.
94. Jokinen M, Rahiala H, Rosenholm JB, Peltola T, Kangasniemi I. Relation between aggregation and heterogeneity of obtained structure in sol-gel derived CaO-P2O5-SiO2. Journal of Sol-Gel Science and Technology 1998;12(3):159-167.
95. Peltola T, Jokinen M, Rahiala H, Patsi M, Heikkila J, Kangasniemi I, Yli-Urpo A. Effect of aging time of sol on structure and in vitro calcium phosphate formation of sol-gel-derived titania films. Journal of Biomedical Materials Research 2000;51(2):200-208.
96. Gan L, Pilliar R. Calcium phosphate sol-gel-derived thin films on porous-surfaced implants for enhanced osteoconductivity. Part I: Synthesis and characterization. Biomaterials 2004;25(22):5303-12.
97. Gil-Albarova J, Garrido-Lahiguera R, Salinas AJ, Roman J, Bueno-Lozano AL, Gil-Albarova R, Vallet-Regi M. The in vivo performance of a sol-gel glass and a glass-ceramic in the treatment of limited bone defects. Biomaterials 2004;25(19):4639-45.
98. Bowers KT, Keller JC, Randolph BA, Wick DG, Michaels CM. Optimization of surface micromorphology for enhanced osteoblast responses in vitro. Int J Oral Maxillofac Implants 1992;7(3):302-10.
99. Keller JC, Stanford CM, Wightman JP, Draughn RA, Zaharias R. Characterizations of titanium implant surfaces. III. J Biomed Mater Res 1994;28(8):939-46.
100. Boyan BD, Bonewald LF, Paschalis EP, Lohmann CH, Rosser J, Cochran DL, Dean DD, Schwartz Z, Boskey AL. Osteoblast-mediated mineral deposition in culture is dependent on surface microtopography. Calcif Tissue Int 2002;71(6):519-29.
101. Cohen J. Tissue reactions to metals—the influence of surface finish. J Bone Joint Surg Am 1961;43:687-99.
102. Carlsson L, Rostlund T, Albrektsson B, Albrektsson T. Removal torques for polished and rough titanium implants. Int J Oral Maxillofac Implants 1988;3(1):21-4.
103. Buser D, Schenk RK, Steinemann S, Fiorellini JP, Fox CH, Stich H. Influence of surface characteristics on bone integration of titanium implants. A histomorphometric study in miniature pigs. J Biomed Mater Res 1991;25(7):889-902.
104. Larsson C, Thomsen P, Aronsson BO, Rodahl M, Lausmaa J, Kasemo B, Ericson LE. Bone response to surface-modified titanium implants: studies on the early tissue response to machined and electropolished implants with different oxide thicknesses. Biomaterials 1996;17(6):605-16.
105. Wennerberg A, Albrektsson T, Ulrich H, Krol JJ. An Optical 3-Dimensional Technique for Topographical Descriptions of Surgical Implants. Journal of Biomedical Engineering 1992;14(5):412-418.

106. Wennerberg A, Ektessabi A, Albrektsson T, Johansson C, Andersson B. A 1-year follow-up of implants of differing surface roughness placed in rabbit bone. Int J Oral Maxillofac Implants 1997;12(4):486-94.
107. Wennerberg A, Albrektsson T, Lausmaa J. Torque and histomorphometric evaluation of c.p. titanium screws blasted with 25- and 75-microns-sized particles of Al2O3. J Biomed Mater Res 1996;30(2):251-60.
108. Wennerberg A, Albrektsson T, Johansson C, Andersson B. Experimental study of turned and grit-blasted screw-shaped implants with special emphasis on effects of blasting material and surface topography. Biomaterials 1996;17(1):15-22.
109. Wennerberg A, Albrektsson T, Andersson B, Krol JJ. A histomorphometric and removal torque study of screw-shaped titanium implants with three different surface topographies. Clin Oral Implants Res 1995;6(1):24-30.
110. Wennerberg A, Albrektsson T. Suggested guidelines for the topographic evaluation of implant surfaces. Int J Oral Maxillofac Implants 2000;15(3):331-44.
111. Webster TJ, Siegel RW, Bizios R. Osteoblast adhesion on nanophase ceramics. Biomaterials 1999;20(13):1221-7.
112. Webster TJ, Ejiofor JU. Increased osteoblast adhesion on nanophase metals: Ti, Ti6Al4V, and CoCrMo. Biomaterials 2004;25(19):4731-9.
113. Webster TJ, Ergun C, Doremus RH, Siegel RW, Bizios R. Specific proteins mediate enhanced osteoblast adhesion on nanophase ceramics. J Biomed Mater Res 2000;51(3):475-83.
114. Webster TJ, Ergun C, Doremus RH, Siegel RW, Bizios R. Enhanced functions of osteoblasts on nanophase ceramics. Biomaterials 2000;21(17):1803-10.
115. de Oliveira PT, Nanci A. Nanotexturing of titanium-based surfaces upregulates expression of bone sialoprotein and osteopontin by cultured osteogenic cells. Biomaterials 2004;25(3):403-13.
116. Brunette DM, Kenner GS, Gould TR. Grooved titanium surfaces orient growth and migration of cells from human gingival explants. J Dent Res 1983;62(10):1045-8.
117. Clark P, Connolly P, Curtis AS, Dow JA, Wilkinson CD. Topographical control of cell behaviour. I. Simple step cues. Development 1987;99(3):439-48.
118. Wojciak-Stothard B, Curtis A, Monaghan W, MacDonald K, Wilkinson C. Guidance and activation of murine macrophages by nanometric scale topography. Exp Cell Res 1996;223(2):426-35.
119. Curtis A, Wilkinson C. Topographical control of cells. Biomaterials 1997;18(24):1573-83.
120. Flemming RG, Murphy CJ, Abrams GA, Goodman SL, Nealey PF. Effects of synthetic micro- and nano-structured surfaces on cell behavior. Biomaterials 1999;20(6):573-88.
121. Dalby MJ, Yarwood SJ, Riehle MO, Johnstone HJ, Affrossman S, Curtis AS. Increasing fibroblast response to materials using nanotopography: morphological and

genetic measurements of cell response to 13-nm-high polymer demixed islands. Exp Cell Res 2002;276(1):1-9.
122. Dalby MJ, Riehle MO, Johnstone H, Affrossman S, Curtis AS. In vitro reaction of endothelial cells to polymer demixed nanotopography. Biomaterials 2002;23(14):2945-54.
123. Andersson AS, Backhed F, von Euler A, Richter-Dahlfors A, Sutherland D, Kasemo B. Nanoscale features influence epithelial cell morphology and cytokine production. Biomaterials 2003;24(20):3427-36.
124. Rice JM, Hunt JA, Gallagher JA, Hanarp P, Sutherland DS, Gold J. Quantitative assessment of the response of primary derived human osteoblasts and macrophages to a range of nanotopography surfaces in a single culture model in vitro. Biomaterials 2003;24(26):4799-818.
125. Riehle MO, Dalby MJ, Johnstone H, MacIntosh A, Affrossman S. Cell behaviour of rat calvaria bone cells on surfaces with random nanometric features. Materials Science & Engineering C-Biomimetic and Supramolecular Systems 2003;23(3):337-340.
126. Dalby MJ, McCloy D, Robertson M, Agheli H, Sutherland D, Affrossman S, Oreffo RO. Osteoprogenitor response to semi-ordered and random nanotopographies. Biomaterials 2006;27(15):2980-7.
127. Zhu XL, Eibl O, Berthold C, Scheideler L, Geis-Gerstrofer J. Structural characterization of nanocrystalline hydroxyapatite and adhesion of pre-osteoblast cells. Nanotechnology 2006;17(11):2711-2721.
128. Sato M, Sambito MA, Aslani A, Kalkhoran NM, Slamovich EB, Webster TJ. Increased osteoblast functions on undoped and ytrrium-doped nanocrystalline hydroxyapatite coatings on titanium. Biomaterials 2006;27(11):2358-69.
129. Albrektsson T, Albrektsson B. Microcirculation in grafted bone. A chamber technique for vital microscopy of rabbit bone transplants. Acta Orthop Scand 1978;49(1):1-7.
130. SPIP™. User's and reference guide version 3.3. Image Metrology.
131. Stout K-J SP, Dong WP, Mainsah E, Luo N, Mathia T, Zahouani H. The development of methods for characterization of roughness in three dimensions. EUR 15178 EN of commision of the European Communities, University of Birmingham, Birmingham 1993.
132. Donath K. Preparation of histologic sections by cutting–grinding technique for hard tissue and other materials not suitable to be sectioned by routine methods. Norderstedt: Exakt-Kulzer publ.; 1993. 1-16P p.
133. Dong W, Mainsah E, Sullivan P, Stout K-J. Instruments ans measurements techniques of 3 dimensional surface topography. In: K-J S, editor. Three dimensional surface topography; measurement, interpetration and applications. London: Penton Press; 1994. p 3-63.
134. Arvidsson A, Sater BA, Wennerberg A. The role of functional parameters for topographical characterization of bone-anchored implants. Clin Implant Dent Relat Res 2006;8(2):70-6.

135. Johansson CB, Morberg P. Importance of ground section thickness for reliable histomorphometrical results. Biomaterials 1995;16(2):91-5.
136. Sul YT. On the bone response to oxidised titanium implants: the role of micro-porous structure and chemical composition of the surface oxide in enhanced osseointegration [PhD]. Göteborg: Göteborg University; 2002.
137. Murugan R, Ramakrishna S. Aqueous mediated synthesis of bioresorbable nanocrystalline hydroxyapatite. Journal of Crystal Growth 2005;274(1-2):209-213.
138. Hench LL. Bioceramics - from Concept to Clinic. Journal of the American Ceramic Society 1991;74(7):1487-1510.
139. Zhu X, Eibl O, Scheideler L, Geis-Gerstorfer J. Characterization of nano hydroxyapatite/collagen surfaces and cellular behaviors. J Biomed Mater Res A 2006;79(1):114-27.